applied sciences

MDPI

Article

Metabolite Profiling of *Christia vespertilionis* Leaf Metabolome via Molecular Network Approach

Anis Irfan Norazhar [1], Soo Yee Lee [1], Siti Munirah Mohd Faudzi [1,2] and Khozirah Shaari [1,2,*]

[1] Natural Medicines and Products Research Laboratory (NaturMeds), Institute of Bioscience, Universiti Putra Malaysia, Serdang 43400, Selangor, Malaysia; anisirfan1512@gmail.com (A.I.N.); leesooyee@upm.edu.my (S.Y.L.); sitimunirah@upm.edu.my (S.M.M.F.)

[2] Department of Chemistry, Faculty of Science, Universiti Putra Malaysia, Serdang 43400, Selangor, Malaysia

* Correspondence: khozirah@upm.edu.my; Tel.: +60-3-8942148

Abstract: *Christia vespertilionis* (L.f.) Bakh. f. is an ornamental plant with unique butterfly-shaped leaves, hence its vernacular name "butterfly wing" or "rerama" in Malay. In Malaysia, the green-leafed variety of this plant has gained popularity in recent years due to testimonial reports by local consumers of its medicinal uses, which include treatment for cancer. Despite these popular uses, there is very limited information on the phytochemistry of the leaf of this plant, presenting a significant gap in the cheminformatics of the plant species. Herein, we report a substantially detailed phytochemical profile of the leaf metabolome of the green-leafed variety of *C. vespertilionis*, obtained by deploying an untargeted tandem mass spectrometry-based molecular networking approach. The detailed inspection of the molecular network map generated for the leaf metabolome enabled the putative identification of 60 metabolites, comprising 13 phenolic acids, 20 flavonoids, 2 benzyltetrahydroisoquinoline-type alkaloids, 4 hydroxyjasmonic acid derivatives, 2 phenethyl derivatives, 3 monoacylglycerols, 4 fatty acid amides, 2 chlorophyll derivatives, 4 carotenoids, 2 organic acids, 1 nucleoside, and 3 amino acids. Flavonoids are the major class of metabolites that characterize the plant leaves. Employing a mass-targeted isolation approach, two new derivatives of apigenin-6-*C*-*β*-glucoside, the major constituents of the plant leaf, were successfully purified and spectroscopically characterized as apigenin-6-*C*-*β*-glucoside 4′-*O*-*α*-apiofuranoside (**28**) and apigenin-6-*C*-*β*-[(4″,6″-*O*-dimalonyl)-glucoside] 4′-*O*-*α*-apiofuranoside (**47**). This work provides further information on the chemical space of the plant leaf, which is a prerequisite to further research towards its valorization as a potential phytopharmaceutical product.

Keywords: *Christia vespertilionis*; global metabolite profiling; LC-MS/MS; molecular network; flavonoids; apigenin-6-*C*-*β*-glucosides

Citation: Norazhar, A.I.; Lee, S.Y.; Faudzi, S.M.M.; Shaari, K. Metabolite Profiling of *Christia vespertilionis* Leaf Metabolome via Molecular Network Approach. *Appl. Sci.* **2021**, *11*, 3526. https://doi.org/10.3390/app11083526

Academic Editor: Gregorio Peron

Received: 23 February 2021
Accepted: 16 March 2021
Published: 15 April 2021

1. Introduction

Since time immemorial, humans have relied on plants as the main source of therapeutic agents for the treatment of various kinds of diseases and maintaining their health. Precious ethnomedicinal knowledge of the diverse plant resources used by different cultures around the world has been passed on over many generations. Despite the exponential growth of synthetic drugs in modern medicine, the practice of using herbs and herbal formulations as alternative medicine has seen a significant upsurge globally due to their availability, cost efficiency, and safety claims [1]. Statistically, it has been estimated that four billion people living in developing countries (80% of the world's population) still depend on herbal medicine as their primary healthcare source [2]. In recent years, multiple product forms derived from plant materials, ranging from supplements, health drinks or tonics, teas, massage oil, and many other forms, have flooded the nutraceutical and herbal supplement markets across the world, catering to the demand and preferences of consumers. Malaysia is of no exception; the use of herbal-based products has become quite the norm [3], marketed as over-the-counter products in pharmacies or via direct selling and network marketing.

Christia vespertilionis (L.f.) Bakh. f. (Family: Fabaceae) is a common ornamental plant, popular for its unique leaf shape and color. The vernacular names given to this small garden plant, "rerama", "mariposa", or "butterfly wings", allude to the unique shape of its terminal leaflet, which looks like the wings of a butterfly. The plant species, originally found in tropical South East Asia regions, exists as two varieties, viz., the red-leafed variety and the green-leafed variety. Other than being grown for ornamental purposes, there have been records of its use in traditional medicine for treating diverse ailments and injuries, including tuberculosis, bronchitis, cold, muscle weakness, poor blood circulation, snake bites, bone fractures, and scabies [4]. Several investigations have reported that the plant possesses antiproliferative, cytotoxic, antimalarial, antidiabetic, and antioxidant properties [5–11]. From the viewpoint of the phytochemistry of this plant in general, it has been reported to contain alkaloids, triterpenes, fatty acids, phenols, alkanes, and long-chained alcohols [4,8,10,11]. Following up on the use of the plant to treat malarial fever, the bicyclic hydrocarbon 7-isopropylidene-1-methyl-1,2,6,7,8,9-hexahydronaphthalene (or christene) has been identified as the potential bioactive principle based on its in vitro antiplasmodial activity [9].

In Malaysia, the use of the green-leafed variety of this plant has risen in popularity, following several testimonials from consumers on the efficacy of the water decoction of the plant leaves in "treating cancer". Despite its popular use, very little is known about the phytochemical constituents of the leaf metabolome of this plant. Thus, considering the medical interest in the plant leaves and from the perspective of quality control, whether for product manufacturing or regulatory purposes, a better understanding of the chemical profile of the leaf metabolome is a logical and important extension to the research and development activities that should be conducted on this plant.

Recent years have witnessed the application of many technological advances in the field of natural product research. This has accelerated and increased the success rate of the discovery of compounds from nature. In the context of untargeted tandem mass spectrometry analysis, various bioinformatics tools, such as iMet [12], MS^n spectral trees [13], and MAGMa (MS annotation based on in silico generated metabolites) [14], have been introduced. These tools are continuously and increasingly being improved to meet the challenges of Big Data analysis, primarily to enable more and more comprehensive chemical interpretation of the vast amount of MS/MS datasets over time. Recently, molecular networking (MN) has emerged as the most versatile and effective tool to organize and mine large datasets acquired from untargeted tandem mass spectrometry (MS/MS) experiments [15]. Unlike many previous tools, MN allows the grouping of compounds into molecular families based on the key concept that structurally similar compounds share similar MS/MS fragmentation patterns, in which the output dataset can be visualized as the mapping of structurally related compounds [16]. With this specialty, MN offers unparalleled visual chemical exploration and dereplication of complex biological extracts, as well as the identification of unknown compounds with known chemical scaffolds that are present and detectable from MS/MS experiments [17].

The present study was undertaken with the primary objective of mapping the chemical space within the leaf metabolome of the green-leafed variety of *C. vespertilionis*. To achieve this goal, detailed phytochemical profiling of the methanolic leaf extract of the green-leafed variety of *C. vespertilionis* was performed using an ultra-high performance liquid chromatography coupled with tandem mass spectrometry (UHPLC-MS/MS)-based molecular networking approach. A mass targeted isolation of two unknown major constituents was also conducted in an attempt to validate their proposed structures. Herein, we report the results of our investigations on the putative identification of chemical constituents in the green-leafed variety of *C. vespertilionis*, highlighting the structural diversity within the molecular families in the leaf metabolome of the plant species.

2. Materials and Methods

2.1. Chemicals and Reagents

Solvents such as hexane, chloroform, ethyl acetate, and methanol were of analytical grade and purchased from Fisher Scientific, Malaysia. Deionized water was purified using the Milli-Q system (supplied by Millipore, Bedford, MA, USA). HPLC grade and LCMS grade solvents were purchased from Merck (Burlington, MA, USA). LCMS grade formic acid was purchased from Sigma Chemical Co. (St. Louis, MO, USA), while deuterated methanol (CD_3OD) was purchased from Merck (Burlington, MA, USA).

2.2. Plant Collection and Sample Preparation

Christia vespertilionis (L.f.) Bakh. f. was obtained from Rimbun Nursery, located in Skudai, Johor, Malaysia, in September 2018. The plant was authenticated by Dr. Mohd Firdaus Ismail, and the voucher specimen (MFI 0150/20) was deposited in the herbarium unit of the Institute of Bioscience, Universiti Putra Malaysia. The fresh leaves of *C. vespertilionis* were washed under running tap water, patted dry with tissue paper, and further dried in a circulating air oven, temperature set to 40 °C, until constant weight. The dried leaves were then ground into fine powder using a mechanical blender (Philips, HR2056, Eindhoven, Netherlands) and stored in an airtight container at 4 °C prior to use.

2.3. Extraction

The powdered leaf material (100 g) was extracted with methanol in a measured volume of solvent (plant-to-solvent ratio of 1:10) by ultrasonic-assisted extraction on a Thermo-10D Ultrasonic Waterbath (Fisher Scientific, Waltham, MA, USA) for 30 min. The bath temperature was maintained between 30 to 40 °C during the sonication. The extraction procedure was repeated using several batches of fresh solvent until the color of the extract produced became light green. The methanolic extracts produced from each batch were pooled and filtered through Whatman filter paper No. 1 (GE Healthcare, Pittsburgh, PA, USA), and subjected to solvent removal via a rotary evaporator (Heidolph Instruments GmbH & Co. KG, Schwabach, Germany), maintaining temperature control at 40 °C.

2.4. UHPLC-MS/MS Analysis

Ultra-high performance liquid chromatography–tandem mass spectrometry (UHPLC-MS/MS) was used to profile the metabolites in *Christia vespertilionis* leaves. For sample preparation, 5 mg of the methanolic extract was dissolved in 1 mL of LCMS grade methanol and filtered through a 0.22 µm hydrophobic PTFE membrane (Sartorius AG, Goettingen, Germany) filter. The UHPLC-MS/MS analysis was performed on a Thermo Fisher Scientific™ Model Q Exactive™ Hybrid Quadrupole-Orbitrap mass spectrometer (San Jose, CA, USA) equipped with a heated electrospray ionization (HESI) source coupled with a surveyor HPLC binary pump, a surveyor diode array detector (DAD; 200–600 nm range, 5 nm bandwidth), and an automatic sample injector. An aliquot of 2 µL of sample was injected for measurement. LC separation was performed on an Acquity BEH C_{18} UPLC column (1.7 µm, 150 × 2.1 mm i.d.; Waters Corporation, Worcester County, MA, USA). The mobile phase for LC separation was composed of a water:acetonitrile (solvent A:solvent B) system, each solvent dosed with 0.1% formic acid. The mobile phase was delivered at a flow rate of 0.4 mL/min, according to the following gradient sequence of percentage solvent B increments: maintained 5% from 0 to 0.5 min, increased from 5 to 100% from 0.5 to 30.0 min, maintained at 100% until 36.0 min. MS/MS analysis was performed in both positive and negative ion modes, with the following optimized operating conditions: spray voltage, 3.5 (+) and 2.5 (−) kV; column temperature, 40 °C; capillary temperature, 262.5 °C; sheath gas flow rate (N_2) at 50 units; auxiliary gas flow rate at 12.5 units; spare gas flow rate at 2.5; S-Lens RF level 45; scan range 150–1200 m/z; collision-induced dissociation (CID) energy was adjusted to 30%. All data were recorded and processed using Thermo Xcalibur Qual Browser software 4.0.

2.5. Generation of Molecular Network

Raw data files acquired from the UHPLC-MS/MS analysis were first converted into mzXML format using the ProteoWizard tool of MSConvertGUI software (version 3.0.11781). The converted data were then uploaded onto the GNPS web platform (http://gnps.ucsd.edu, accessed on 20 December 2019) using the FTP server (FileZilla, https://filezilla-project.org/, accessed on 20 December 2019) for the generation of molecular networks. The uploaded MS/MS spectra datasets were then clustered with the aid of MS-Cluster to create consensus spectra. The consensus spectra were created from a precursor ion mass tolerance of 0.02 Da and a fragment ion mass tolerance of 0.02 Da. Each spectral network was then created based on the following parameters: a minimum of six matched fragment ions between the consensus spectra, a minimum cosine score value of 0.7, and network topK of 10. For the dereplication process, each of the spectra in the network was searched against GNPS spectral libraries. The automated spectral library matching required the spectra to have a minimum of six matched fragment ions. The generated molecular network was visualized using Cytoscape software (version 3.6.0). To avoid misinterpretation of HPLC-contaminants or noise, a blank solvent (methanol) injection was also included in the spectral network as a distinct sample group.

2.6. Semiquantitative Analysis

The semiquantitative analysis of the identified compounds in *C. vespertilionis* methanolic leaf extract was performed on the basis of the peak area calculation procedure, which reports the area of each peak from the extracted ion chromatogram (XIC) as a percentage of the total area of all identified peaks. Prior to the calculation procedure, the mzXML format of the UHPLC-MS/MS raw data was subjected to series of data treatment steps (mass detection, chromatogram builder, peak deconvolution, isotopic filtering, and peak alignment), processed using Mzmine software (version 2.31).

2.7. Fractionation and MS-Targeted Isolation of Compounds **28** and **47**

The crude extract (23.86 g) was reconstituted in a methanol:water (1:2) solvent system and subjected to liquid–liquid solvent partitioning using solvents of increasing polarity (n-hexane, chloroform, and ethyl acetate). Owing to the typical solubility of the chemical class of the targeted compounds in ethyl acetate [18,19], the ethyl acetate soluble fraction obtained was evaporated to dryness via rotary evaporator, with the temperature maintained at 40 °C, to yield 0.36 g of dried fraction, which was further subjected to isolation using semipreparative high performance liquid chromatography (semiprep HPLC). Separation of the chemical constituents was achieved using an XBridge™ C_{18} column (5 µm, 150 × 10 mm i.d.; Waters Corporation, USA), operated on a JASCO liquid chromatography system equipped with JASCO PU-2086 Plus Intelligent preparative pumps and a JASCO UV-2077 Plus 4-wavelength Intelligent UV/VIS DAD detector, using a water:acetonitrile (solvent A:solvent B) solvent system as the mobile phase, with a flow rate of 3 mL/min. The optimized mobile phase composition for the separation was set according to the following gradient sequence of percentage solvent B increments: 10–15% for 0–25 min, 15–25% for 25–30 min, 25–30% for 30–40 min, 30–100% for 40–50 min, maintained at 100% until 52 min. The chromatogram was monitored at 254 nm, and the targeted compounds were manually collected as they eluted from the column at their respective retention times. The structures of the isolated compounds were further analyzed by 1D (^{1}H with water presaturation at 700 MHz) and 2D NMR experiments (HSQC, HMBC, and TOCSY) recorded on a Bruker Ascend 700 MHz spectrometer (Bruker Bio spin, Germany) equipped with a TCI cryoprobe. The 2D NMR spectra were recorded using regular pulse sequences. For data analysis, the FID files were processed with MestReNova version 6.0.2-5475 (Mestrelab Research, Santiago de Compostela, Spain), while chemical shifts were reported in parts per million (δ), relative to the signal of the internal standard, tetramethylsilane (TMS). All experiments were performed in deuterated methanol (CD_3OD). The ^{13}C chemical shift

data of the isolated compounds were gleaned from HSQC (^{1}J correlations) and HMBC ($^{2\text{-}3}J$ correlations).

3. Results and Discussion

3.1. Metabolite Profiling of the Leaf Metabolome of the Green-Leafed Variety of Christia vespertilionis via Untargeted Tandem Mass Spectrometry-Based Molecular Networking

The UHPLC-MS/MS spectral data of the methanolic leaf extract of *C. vespertilionis* was successfully acquired as the first step towards establishing a detailed phytochemical composition of the leaf metabolome. More than 300 MS/MS spectra over the mass range of m/z 120 to 1500 were generated in both positive and negative ion modes. The respective total ion chromatograms (TICs) and photodiode array chromatograms (PDAs) obtained are presented in Figure S1a,b . The plant leaves' chemical space was further analyzed in detail by mapping structurally related compounds into molecular networks. To achieve this, the acquired large datasets of MS/MS fragmentation spectra were processed and organized as molecular networks (MNs) according to the online workflow provided by the Global Natural Products Social Molecular Networking (GNPS) platform (http://gnps.ucsd.edu, accessed on 20 December 2019). The MNs generated from the mass spectral data of the extract are depicted in Figure 1, where the consensus MS/MS spectrum of each detected molecular ions, generated by the aid of the MS-Cluster algorithm, was visualized as a node (blue circles), while the edge (grey lines) connecting the nodes indicated that they possess a homologous MS/MS fragmentation pattern, hence, allowing them to be mapped together within the same cluster (node $\geq$ 2) as a molecular family.

Visual inspection of this generated molecular network map permitted the annotation of various clusters of metabolites comprising phenolic acids, mono- and dihydroxyflavones, *C*-glycosylflavone derivatives, flavonol 3-*O*-glycosides, benzyltetrahydroisoquinoline-type alkaloids, hydroxyjasmonic acid derivatives, phenethyl derivatives, monoacylglycerols, fatty acid amides, chlorophyll derivatives, and carotenoids, as well as some of the "self-loop" nodes, including organic acids, nucleoside, amino acids, and flavone-*C*,*O*-diglycoside. In brief, a total of 60 metabolites were characterized and tentatively identified based on the diagnostic MS/MS fragment ions, MS/MS spectral data matched with published literatures, structural hits obtained from GNPS spectral library matching, and by interpreting the MS/MS spectra of unknown compounds by comparison to the MS/MS spectra of their close structural analogs (tentative candidates). From these, 58 compounds are reported for the first time in the leaf metabolome of this plant. Notably, 16 of the compounds are proposed as new structures based on a detailed inspection of their MS/MS data, which include 2 derivatives of phenolic acid ester, 2 derivatives of dihydroxybenzoic acid, 2 derivatives of dihydroxyflavone, 4 derivatives of apigenin 6-*C*-glucoside, 2 derivatives of benzyltetrahydroisoquinoline-type alkaloid, 2 derivatives and 1 isomer of hydroxyjasmonic acid, and a derivative of phenethyl. The characteristic fragmentation patterns of the proposed new structures are discussed in detail.

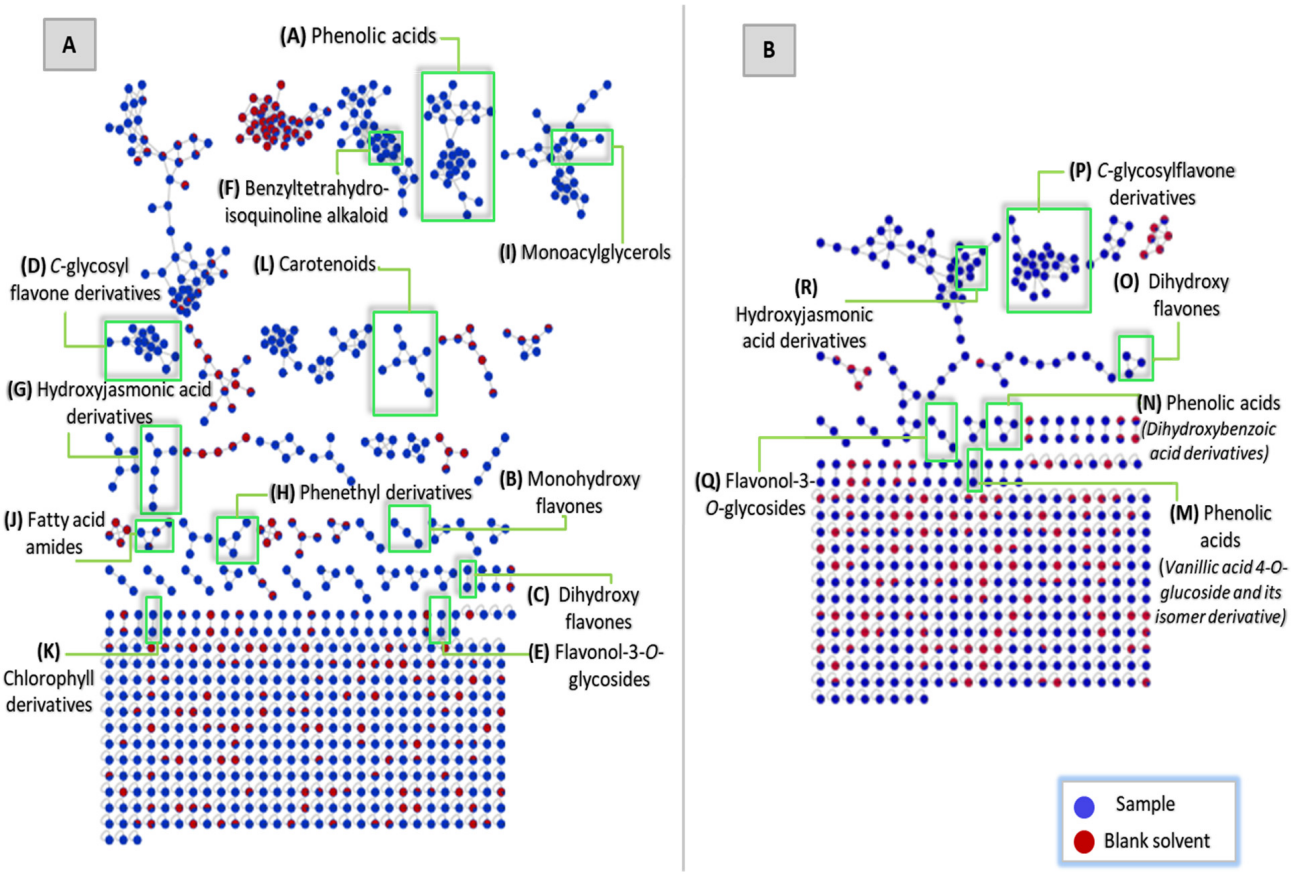

Figure 1. Full visualization of the molecular network for the methanolic leaf extract of *Christia vespertilionis* (green-leafed variety) generated from the (**A**) positive and (**B**) negative ion modes of MS/MS spectral data.

From the results of the semiquantitative analysis, it is worth mentioning that flavonoids were the major class of metabolites in the leaf metabolome, representing 78.48% of the identified metabolites. This was followed by phenolic acids (7.61%), miscellaneous compounds (6.35%), and carotenoids (3.20%). The other chemical classes were present at lower relative percentages. All the identified metabolites, along with their respective retention times (RT), molecular formula, precursor ion (m/z), key fragments data, and relative abundance (%), are listed in Table 1. The following subsections discuss the annotation of the metabolites of selected clusters and "self-loop" nodes mapped in the network.

Table 1. Chemical constituents identified in the methanolic leaf extract of *Christia vespertilionis* (green-leafed variety).

Peak No.	RT (min)	Compound Identification	Molecular Formula	Precursor Ion (*m*/*z*)	Ion Type	Key Fragments (*m*/*z*)	Area	Relative Abundance (%)
Phenolic acids ***(Clusters A, M, N, and "self-loop" nodes)***								
2	1.03	Caffeoyl glucoside [c]	$C_{15}H_{18}O_9$	360.150	$[M + NH_4]^+$	163, 109	2.6×10^8	3.99
6	1.54	Crotonylated derivative of vanillic acid glucosyl ester [d]**	$C_{18}H_{22}O_{10}$	397.075	$[M - H]^-$	329, 122	5.3×10^6	0.08
7	1.63	Caffeoylglycolic acid methyl ester [c]	$C_{12}H_{12}O_6$	270.155	$[M + NH_4]^+$	163, 109	9.4×10^6	0.14
9	2.28	Dihydroxybenzoic acid crotonyl hexoside [d]**	$C_{17}H_{20}O_{10}$	383.059	$[M - H]^-$	315, 153, 152, 109	1.3×10^7	0.20
10	2.32	Vanillic acid 4-*O*-glucoside [c]	$C_{14}H_{18}O_9$	348.129 329.088	$[M + NH_4]^+$ $[M - H]^-$	169, 151 167, 122	6.1×10^6	0.09
11	3.05	*p*-coumaroylquinic acid [c]	$C_{16}H_{18}O_8$	356.155	$[M + NH_4]^+$	175, 131	9.4×10^6	0.14
13	3.68	*p*-hydroxybenzoic acid 4-*O*-glucoside [c]	$C_{13}H_{16}O_8$	318.119	$[M + NH_4]^+$	139, 121	5.8×10^6	0.09
14	3.89	Caffeic acid 4-*O*-glucoside [c]	$C_{15}H_{18}O_9$	360.129	$[M + NH_4]^+$	181, 163	4.6×10^6	0.07
15	3.92	Isopropyl derivative of caffeoylglycolic acid methyl ester [d]**	$C_{14}H_{14}O_7$	312.165	$[M + NH_4]^+$	163, 109	3.9×10^6	0.06
16	3.96	Dihydroxybenzoic acid malonyl hexoside [b]	$C_{16}H_{18}O_{12}$	401.072	$[M - H]^-$	357, 315, 153, 152, 109	6.7×10^6	0.10
17	4.01	*p*-coumaric acid 4-*O*-glucoside [a]	$C_{15}H_{18}O_8$	344.134 325.093	$[M + NH_4]^+$ $[M - H]^-$	165, 147, 119 163	7.2×10^7	1.11
22	4.48	Ferulic acid 4-*O*-glucoside [c]	$C_{16}H_{20}O_9$	374.145 355.103	$[M + NH_4]^+$ $[M - H]^-$	195, 177, 149 193	1.0×10^8	1.54
46	8.07	Dihydroxybenzoic acid dimalonyl hexoside [d]**	$C_{19}H_{20}O_{15}$	487.146	$[M - H]^-$	315, 153, 152, 109	6.7×10^6	0.10
Monohydroxyflavones ***(Cluster B)***								
18	4.08	5 or 7-hydroxyflavone [d]	$C_{15}H_{10}O_3$	239.128	$[M + H]^+$	221, 137, 109, 93	2.1×10^7	0.32
19	4.11	7-hydroxyflavone glucoside [c]	$C_{21}H_{20}O_8$	401.181 418.207	$[M + H]^+$ $[M + NH_4]^+$	239, 221, 137, 109, 93 239, 221, 137, 109, 93	2.0×10^7	0.31
Dihydroxyflavones ***(Clusters C and O)***								
20	4.13	5,7-dihydroxyflavone (Chrysin) [b]	$C_{15}H_{10}O_4$	255.123 253.108	$[M + H]^+$ $[M - H]^-$	237, 209, 177, 153 175, 151	4.9×10^7	0.75
21	4.13	7-*O*-crotonylchrysin [c]**	$C_{19}H_{14}O_5$	321.095	$[M - H]^-$	253, 175, 151	5.8×10^6	0.09
25	5.09	7-*O*-malonylchrysin [c]**	$C_{18}H_{12}O_7$	341.123	$[M + H]^+$	237, 177, 153	4.1×10^6	0.06
C*-glycosylflavone Derivatives** ***(Clusters D and P)								
27	5.23	Luteolin-6-*C*-glucoside (isoorientin) [a]	$C_{21}H_{20}O_{11}$	449.108 447.093	$[M + H]^+$ $[M - H]^-$	329, 287 429, 357, 327, 298, 285	5.5×10^7	0.84

Table 1. *Cont.*

Peak No.	RT (min)	Compound Identification	Molecular Formula	Precursor Ion (*m*/*z*)	Ion Type	Key Fragments (*m*/*z*)	Area	Relative Abundance (%)
28	**5.35**	**Apigenin-6-*C*-*β*-glucoside 4′-*O*-*α*-apiofuranoside ****	**$C_{26}H_{28}O_{14}$**	**565.155** **563.140**	**$[M + H]^+$** **$[M - H]^-$**	**445, 313, 284, 271** **473, 443, 341, 311, 282, 269**	**8.7×10^8**	**13.36**
30	5.60	Apigenin-6,8-di-*C*-glucoside (vicenin 2) [b]	$C_{27}H_{30}O_{15}$	595.166	$[M + H]^+$	433, 337, 367	4.2×10^8	6.45
35	6.00	Apigenin-6-*C*-glucoside (isovitexin) [a]	$C_{21}H_{20}O_{10}$	433.113 431.098	$[M + H]^+$ $[M - H]^-$	361, 313, 284, 271 341, 311, 282, 269	7.9×10^8	12.13
36	6.02	Apigenin-6-*C*-(6″-*O*-dihydroxybenzoyl)- glucoside [d]**	$C_{28}H_{24}O_{13}$	567.073	$[M - H]^-$	413, 341, 311, 282, 269	7.2×10^8	11.06
37	6.05	Apigenin-6-*C*-(6″-*O*-crotonyl)-glucoside [c]**	$C_{25}H_{24}O_{11}$	499.085	$[M - H]^-$	413, 341, 311, 282, 269	6.3×10^8	9.67
38	6.17	Apigenin-8-*C*-glucoside (vitexin) [c]	$C_{21}H_{20}O_{10}$	431.192	$[M - H]^-$	341, 311, 282, 269	3.5×10^7	0.54
40	6.36	Diosmetin-6-*C*-glucoside [b]	$C_{22}H_{22}O_{11}$	463.123 461.109	$[M + H]^+$ $[M - H]^-$	391, 343, 313, 297, 151 371, 341, 312, 299	1.9×10^7	0.29
43	7.13	Apigenin-6-*C*-(6″-*O*-malonyl)-glucoside [c]	$C_{24}H_{22}O_{13}$	519.114 517.098	$[M + H]^+$ $[M - H]^-$	415, 313, 271 413, 341, 311, 282, 269	7.4×10^7	1.14
44	7.13	Apigenin-6-*C*-(6″-*O*-acetyl)-glucoside [c]	$C_{23}H_{22}O_{11}$	473.109	$[M - H]^-$	413, 341, 311, 282, 269	5.9×10^6	0.09
47	**9.36**	**Apigenin-6-*C*-*β*-[(4″,6″-*O*-dimalonyl)-glucoside] 4′-*O*-*α*-apiofuranoside ****	**$C_{32}H_{32}O_{20}$**	**737.229** **735.214**	**$[M + H]^+$** **$[M - H]^-$**	**313, 284, 271** **545, 473, 443, 341, 311, 282, 269, 249**	**9.8×10^8**	**15.05**
Flavone-*C*,*O*-diglycoside *("self-loop" node)*								
31	5.60	Apigenin-6-*C*-glucosyl-2″-*O*-glucoside (isovitexin-2″-*O*-glucoside) [b]	$C_{27}H_{30}O_{15}$	593.151	$[M - H]^-$	473, 413, 293	1.2×10^8	1.84
Flavonol-3-*O*-glycosides *(Clusters E and Q)*								
34	5.86	Quercetin-3-*O*-rutinoside (Rutin) [a]	$C_{27}H_{30}O_{16}$	611.161 609.146	$[M + H]^+$ $[M - H]^-$	465, 303 301, 300, 271, 255, 179, 151	2.1×10^8	3.22
39	6.21	Quercetin-3-*O*-glucoside (Isoquercitrin) [a]*	$C_{21}H_{20}O_{12}$	463.088	$[M - H]^-$	301, 300, 271, 255, 179, 151	3.7×10^6	0.06
41	6.36	Kaempferol- 3-*O*-rutinoside [b]	$C_{27}H_{30}O_{15}$	595.166 593.151	$[M + H]^+$ $[M - H]^-$	449, 287 285, 255, 227, 151	4.6×10^7	0.71
Benzyltetrahydroisoquinoline alkaloids *(Cluster F)*								
23	4.51	Benzyltetrahydroisoquinoline derivative [d]**	$C_{22}H_{28}O_4N$	370.170	$[M + H]^+$	299, 145, 127	4.9×10^7	0.75
29	5.56	Benzyltetrahydroisoquinoline derivative [d]**	$C_{21}H_{26}O_3N$	340.160	$[M + H]^+$	269, 175, 145, 127, 119	3.3×10^7	0.51

Table 1. *Cont.*

Peak No.	RT (min)	Compound Identification	Molecular Formula	Precursor Ion (*m*/*z*)	Ion Type	Key Fragments (*m*/*z*)	Area	Relative Abundance (%)
Hydroxyjasmonic acid derivatives *(Clusters G and R)*								
24	4.71	3-oxo-2-[5-(hexopyranosyloxy)-pent-2-enyl]-cyclopentaneacetic acid (Tuberonic acid hexoside) [a]	$C_{18}H_{28}O_9$	406.207 387.166	$[M + NH_4]^+$ $[M - H]^-$	227, 209, 163 207, 59	1.7×10^7	0.26
26	5.08	Hydrogenated derivative of tuberonic acid hexoside [c**]	$C_{18}H_{30}O_9$	408.223 389.182	$[M + NH_4]^+$ $[M - H]^-$	229, 211, 165 209, 59	5.7×10^6	0.09
33	5.75	Tuberonic acid hexoside isomer [d**]	$C_{18}H_{28}O_9$	406.244	$[M + NH_4]^+$	209, 163	9.4×10^6	0.14
42	6.81	Malonylated derivative of tuberonic acid hexoside isomer [d**]	$C_{21}H_{30}O_{12}$	492.244 475.217	$[M + NH_4]^+$ $[M + H]^+$	227, 209, 163 227, 209, 163	7.4×10^6	0.11
Phenethyl derivatives *(Cluster H)*								
32	5.68	Phenethyl 1-*O*-*β*-D-apiofuranosyl (1→2)-*β*-D-glucopyranoside (Sayaendoside) [a]	$C_{19}H_{28}O_{10}$	434.202	$[M + NH_4]^+$	295, 133, 123	5.6×10^6	0.09
45	7.56	Isopropyl derivative of phenethyl 1-*O*-*β*-D-apiofuranosyl (1→2)-*β*-D-glucopyranoside [d**]	$C_{22}H_{34}O_{10}$	476.213	$[M + NH_4]^+$	295, 165, 133	8.2×10^6	0.13
Monoacylglycerols *(Cluster I)*								
48	16.66	6,9,12,15-Octadecatetraenoic acid, 2,3-dihydroxypropyl ester [c]	$C_{21}H_{33}O_3$	351.254	$[M + H]^+$	259, 241	7.5×10^6	0.12
38	6.17	Apigenin-8-*C*-glucoside (vitexin) [c]	$C_{21}H_{20}O_{10}$	431.192	$[M - H]^-$	341, 311, 282, 269	3.5×10^7	0.54
49	19.17	9,12,15-Octadecatrienoic acid, 3-(hexopyranosyl)-2-hydroxylpropyl ester [a]	$C_{27}H_{46}O_9$	532.348	$[M + NH_4]^+$	353, 261, 243	6.8×10^6	0.10
50	22.11	9,12,15-Octadecatrienoic acid, 2,3-dihydroxypropyl ester (1-monolinolenin) [a]	$C_{21}H_{35}O_3$	370.295 353.269	$[M + NH_4]^+$ $[M + H]^+$	353, 261, 243 261, 243	7.1×10^6	0.11
Fatty acid amides *(Cluster J)*								
51	22.82	9,12-octadecadienamide [b]	$C_{18}H_{33}NO$	280.264	$[M + H]^+$	263, 245	1.5×10^6	0.02
52	24.80	9-octadecenamide [b]	$C_{18}H_{35}NO$	282.279	$[M + H]^+$	265, 247	5.6×10^7	0.86
55	27.12	9-eicosenoic acid formamide [b]	$C_{20}H_{39}NO$	310.310	$[M + H]^+$	293, 275	4.2×10^6	0.06
60	29.11	13-docosenamide [b]	$C_{22}H_{43}NO$	338.342	$[M + H]^+$	321, 303	3.6×10^7	0.55
Chlorophyll derivatives *(Cluster K)*								
53	25.88	Pheophorbide-a [a*]	$C_{35}H_{36}N_4O_5$	593.277	$[M + H]^+$	533, 459, 447	2.0×10^7	0.31
56	27.98	Pheophorbide-a methyl ester [c]	$C_{36}H_{38}N_4O_5$	607.292	$[M + H]^+$	575, 487, 447	2.1×10^7	0.32

Table 1. *Cont.*

Peak No.	RT (min)	Compound Identification	Molecular Formula	Precursor Ion (*m*/*z*)	Ion Type	Key Fragments (*m*/*z*)	Area	Relative Abundance (%)
Carotenoids *(Cluster L)*								
54	26.59	Violaxanthin [b]	$C_{40}H_{56}O_4$	601.425	$[M + H]^+$	583, 521, 221, 145, 119	2.6×10^6	0.04
57	28.00	β-apo-12′-luteinal [c]	$C_{25}H_{34}O_2$	367.263	$[M + H]^+$	349, 161, 145, 119	1.2×10^6	0.02
58	28.00	Antheraxanthin [b]	$C_{40}H_{56}O_3$	585.430	$[M + H]^+$	567, 549, 221, 145, 119	3.8×10^7	0.58
59	28.02	Lutein [b]	$C_{40}H_{56}O_2$	568.428	$[M]^{\bullet+}$	430, 145, 135, 119	1.8×10^8	2.76
Miscellaneous compounds *("self-loop" nodes)*								
Organic acids								
1	0.90	D-Gluconic acid [b]	$C_6H_{12}O_7$	195.050	$[M - H]^-$	177, 147, 129, 111	3.2×10^8	4.91
4	1.18	Citric acid [b]	$C_6H_8O_7$	191.019	$[M - H]^-$	173, 129, 111	8.3×10^6	0.13
Nucleoside								
3	1.18	Adenosine [b]	$C_{10}H_{13}N_5O_4$	268.104	$[M + H]^+$	136, 119	4.0×10^7	0.61
Amino acids								
5	1.21	Tyrosine [b]	$C_9H_{11}NO_3$	182.081	$[M + H]^+$	165, 136, 119	6.8×10^6	0.10
8	2.19	Phenylalanine [b]	$C_9H_{11}NO_2$	166.086	$[M + H]^+$	120, 103	2.1×10^7	0.32
12	3.21	Tryptophan [b]	$C_{11}H_{12}N_2O_2$	205.097	$[M + H]^+$	188, 159	1.8×10^7	0.28

Peak numbers correspond to the numbering of peaks that appear in total ion chromatograms (TICs) (Figure S1a). [a] Structural hit obtained from GNPS spectral library matching. [b] MS/MS spectra matched with published literature. [c] Annotated based on diagnostic fragment ions. [d] Tentative candidate. * Compounds previously reported in *C. vespertilionis* according to Dash [4]. ** Proposed new structures. Compounds in bold letters (Peaks 28 and 47) were further isolated and elucidated by 1D and 2D NMR experiments.

3.1.1. Phenolic Acids

Visual inspection of the generated MNs in both ion modes revealed the presence of 3 distinct clusters (A, M, and N) and 2 "self-loop" nodes belonging to phenolic acids (Figure 2). In negative ion mode, the classification of these compounds was more specific since the different types of subgroups of the phenolic acids were separated from each other.

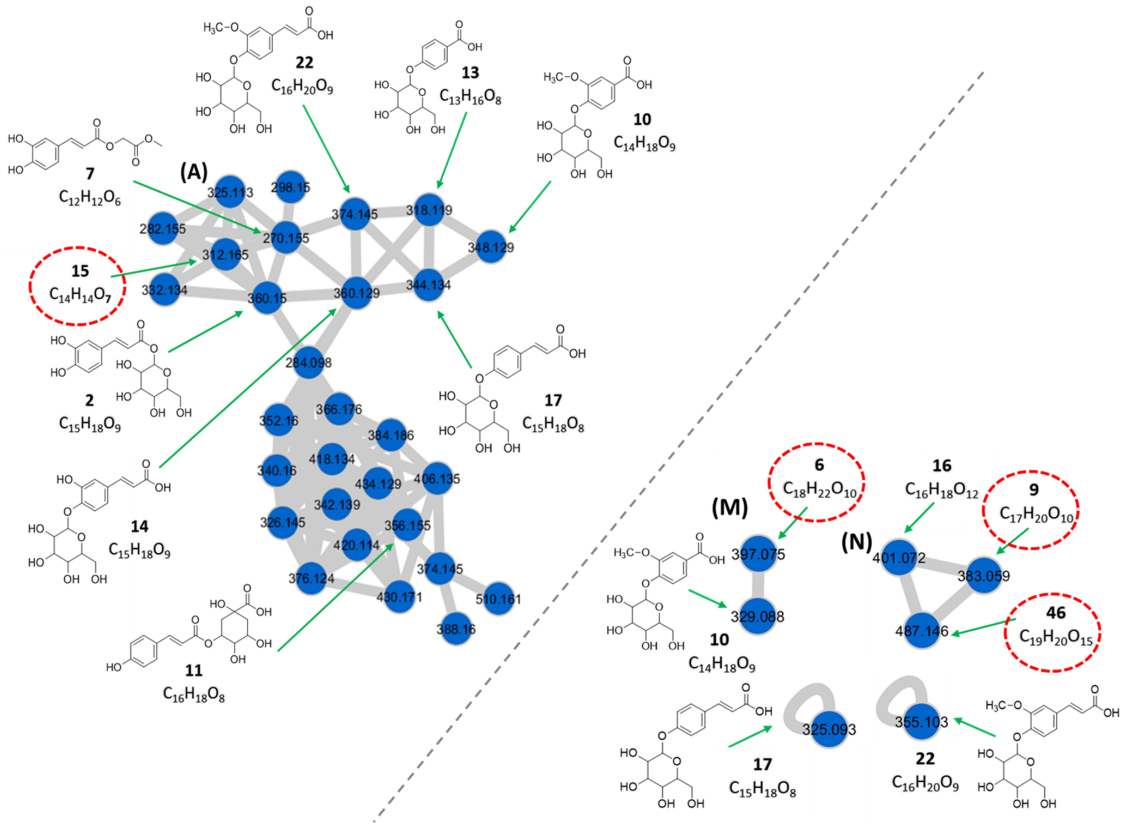

Figure 2. Molecular family of phenolic acids putatively identified from Cluster **A** in positive ion mode and Clusters **M**, **N**, and "self-loop" nodes in negative ion mode. Red dotted circles represent proposed new structures.

Initially, automated GNPS spectral library matching on the spectral node in Cluster A with a precursor ion at m/z 344.134 $[M + NH_4]^+$ permitted the annotation of a known phenolic acid glycoside molecule, namely, *p*-coumaric acid 4-*O*-glucoside. In order to propagate the annotation of the connected nodes forming the molecular family of Cluster A, a detailed inspection of MS/MS fragmentation patterns was carried out. A total of 9 phenolic acids were identified, consisting of phenolic acid esters (**2**, **7**, **11**, and **15**) and phenolic acid glycosides (**10**, **13**, **14**, **17**, and **22**). All the phenolic acids identified in Cluster A were in the form of their ammonium adduct ions, $[M + NH_4]^+$.

The four nodes with precursor ions at m/z 360.150 $[M + NH_4]^+$, 270.155 $[M + NH_4]^+$, 356.155 $[M + NH_4]^+$, and 312.165 $[M + NH_4]^+$ were identified as phenolic acid esters. A node with a precursor ion at m/z 360.150 $[M + NH_4]^+$ was putatively characterized as caffeoyl glucoside (2), the structural isomer of caffeic acid 4-*O*-glucoside (**14**), which differed by the position of glucoside moiety attached to the caffeic acid parent structure. Specifically, its MS/MS data showed the characteristic fragment ion of a dehydrated caffeic acid moiety at m/z 163 for $[(M+NH_4)\text{-}NH_3\text{-}C_6H_{12}O_6]^+$, which resulted from the direct losses of ammonia and an intact glucoside moiety. Furthermore, it also generated a fragment ion assignable to the 3,4-dihydroxyphenyl moiety at m/z 109 for $[(M+NH_4)\text{-}NH_3\text{-}C_6H_{12}O_6\text{-}C_3H_2O]^+$, after losing 54 Da from the transition ion at m/z 163. This was in agreement with the structural characteristic of caffeic acid esterified with one glucoside moiety at the carboxyl group. For the node with a precursor ion at m/z 270.155 $[M + NH_4]^+$,

the compound was identified as caffeoylglycolic acid methyl ester (**7**). The compound showed a fragment ion for a dehydrated caffeic acid moiety at m/z 163 for $[(M+NH_4)\text{-}NH_3\text{-}C_3H_6O_3]^+$, which resulted from the losses of ammonia and a glycolic acid methyl ester moiety and a characteristic 3,4-dihydroxyphenyl fragment ion at m/z 109, all of which provided evidence that the caffeic acid was esterified with a glycolic acid methyl ester moiety. The node with a precursor ion at m/z 356.155 $[M + NH_4]^+$ was characterized as *p*-coumaroylquinic acid (**11**) based on the characteristic fragment ion for a dehydrated quinic acid moiety at m/z 175 for $[(M+NH_4)\text{-}NH_3\text{-}C_9H_8O_3]^+$, which resulted from the losses of ammonia and a coumaroyl moiety, followed by decarboxylation of the carboxylic acid group, giving rise to a fragment ion at m/z 131. Another node with a precursor ion at m/z 312.165 $[M + NH_4]^+$ (**15**), a mass difference of 42 Da from that of **7**, was tentatively proposed as an isopropyl derivative of **7**. Since the MS/MS data of this compound (**15**) exhibited the same characteristic fragment ions as **7** at m/z 163, and 109, for $[(\text{caffeoyl+H})\text{-}H_2O]^+$, and 3,4-dihydroxyphenyl, respectively, it could be suggested that the additional isopropyl substituent (C_3H_6, 42 Da) is directly attached to the carbon chain of the glycolic acid methyl ester moiety.

In addition to the annotated spectral node via the GNPS library, which showed a precursor ion at m/z 344.134 $[M + NH_4]^+$ for *p*-coumaric acid 4-*O*-glucoside (**17**), four other neighboring nodes, showing precursor ions $[M + NH_4]^+$ at m/z 348.129, 318.119, 360.129, and 374.145, were also annotated as known phenolic acid glycoside molecules, namely, vanillic acid 4-*O*-glucoside (**10**), *p*-hydroxybenzoic acid 4-*O*-glucoside (**13**), caffeic acid 4-O-glucoside (**14**), and ferulic acid 4-*O*-glucoside (**22**), respectively. These compounds generated main characteristic fragment ions of their protonated aglycone molecules $[(M+NH_4)\text{-}NH_3\text{-}162]^+$ at m/z 169 (**10**), 139 (**13**), 181 (14), 165 (**17**), and 195 (**22**), which originated from a direct cleavage of the *O*-glycosidic bond (glucoside moiety, 162 Da) and the loss of ammonia. Further loss of one unit of their water molecule and/or successive loss of 46 Da ($CO+H_2O$) from their protonated aglycone molecule were found consistent with the presence of carboxylic acid group within their parent structures. The fragmentation pathway proposed for compound **17** is provided in Figure S2 as a representative example for the common neutral losses observed in the fragmentation of phenolic acid glycoside molecules recorded in positive ion mode. Additionally, the presence of compounds **10**, **17**, and **22** can be further supported by the MS/MS data recorded in negative ion mode, as represented by the nodes at m/z 329.088 $[M - H]^-$, 325.093 $[M - H]^-$, and 355.103 $[M - H]^-$, respectively. These compounds showed the main fragment ion of their deprotonated aglycone molecules $[(M-H)\text{-}162]^-$ at m/z 167 (**10**), 163 (**17**), and 193 (**22**), resulting from a direct cleavage of the *O*-glycosidic bond.

The spectral nodes assigned to Cluster M were classified as vanillic acid 4-*O*-glucoside and a derivative of its structural isomer, which showed precursor ions $[M - H]^-$ at m/z 329.088 (**10**) and 397.075 (**6**), respectively. Compound **10** was characterized as vanillic acid 4-*O*-glucoside, which produces a fragment ion at m/z 167 for $[(M-H)\text{-}162]^-$ due to direct cleavage at the *O*-glycosidic bond. Further decarboxylation and additional loss of proton gave rise to a fragment ion at m/z 122 for $[(M-H)\text{-}162\text{-}COOH]^{-\bullet}$, which was consistent with the MS/MS data reported by Mekky et al. [20]. With a mass difference of 68 Da (C_4H_4O) from that of **10**, along with the presence of identical fragment ions at m/z 329 and 122, the node with a precursor ion $[M - H]^-$ at m/z 397.075 (**6**) was initially proposed as a crotonylated derivative of **10**. However, the absence of a fragment ion at m/z 167 suggested that the parent structure of this compound was a phenolic acid ester, known as vanillic acid glucosyl ester, a structural isomer of **10** (Figure S3). Based on these MS/MS data, this compound was concluded to be a crotonylated derivative of vanillic acid glucosyl ester (**6**) that consisted of two feasible sites for the attachment of the crotonyl moiety (C_4H_4O), either at the hydroxyl group of C-4 or at one of the hydroxyl groups of the glucoside moiety.

A detailed analysis of Cluster N revealed the compounds as dihydroxybenzoic acid derivatives. Through comparisons with literature data [20], the node with a precursor ion

at m/z 401.072 $[M - H]^-$ was subsequently identified as dihydroxybenzoic acid malonyl hexoside (**16**). Moreover, by considering the mass differences of 18 and 86 Da from that of 16, the nodes with precursor ions $[M - H]^-$ at m/z 383.059 and 487.146 were proposed to be crotonylated (C_4H_4O, 68 Da) (**9**) and dimalonylated ($C_6H_4O_6$, 172 Da) (**46**) derivatives of dihydroxybenzoic acid hexoside, respectively. Examination of their MS/MS spectral data showed that they possessed fragmentation patterns that are compatible with the characteristic fragment ion of dihydroxybenzoic acid acyl hexoside (Figures S4 and S5); these were based on the fragment ions at m/z 315 for $[(M-H)\text{-acyl}]^-$, 153 for $[(M-H)\text{-acyl-162}]^-$, 152 for $[(M-H)\text{-acyl-162-H}]^{-\bullet}$, and 109 for $[(M-H)\text{-acyl-162-}CO_2]^-$, resulting from the loss of the acyl hexoside moiety, followed by decarboxylation of the carboxylic acid group.

3.1.2. Flavonoids

A total of 20 compounds were identified as flavonoids, which included mono- and dihydroxyflavones, *C*-glycosylflavone derivatives, flavonol 3-*O*-glycosides, and flavone-*C*,*O*-diglycosides. These compounds were mapped into 4 distinct clusters (B, C, D, and E) based on positive ion mode MS/MS and 3 distinct clusters (O, P, and Q) and one "self-loop" node based on negative ion mode MS/MS, according to their substituent groups and types of glycosidic linkages (Figure 3).

Monohydroxyflavones

Interpretation of the MS/MS spectral data for a node in Cluster B (Figure 3) with a precursor ion $[M + H]^+$ at m/z 239.128 led to the tentative identification of a monohydroxyflavone that could be assigned as 5 or 7-hydroxyflavone (**18**). The MS/MS fragmentation of **18** produced a prominent fragment ion at m/z 137 $[^{1,3}A]^+$, generated from the cleavage of ring-C of the flavone at positions 1 and 3, via the retro-Diels-Alder (RDA) mechanism, thus verifying that the hydroxyl group was attached to ring-A. Other fragment ions exhibited at m/z 221 for $[(M+H)\text{-}H_2O]^+$, 109 for $[^{1,3}A\text{-}CO]^+$, and 93 for $[^{O,4}A]^+$ further support this suggested structure. For the node with a precursor ion $[M + H]^+$ at m/z 401.181, the compound differed from **18** by 162 Da, indicating that a sugar moiety (hexose) is present within its parent structure. This compound (**19**) showed similar fragment ions as **18**, i.e., at m/z 239, 221, 137, 109, and 93 (Figure S6), suggesting that the aglycone moiety could also be a 5 or 7-hydroxyflavone. A base peak ion observed at m/z 239 for $[(M+H)\text{-}162]^+$, due to the direct loss of sugar moiety, suggested an *O*-glycosylation of the phenolic hydroxyl group of **19**. Since 5-OH substituent on a flavonoid structure has very low reactivity towards glycosylation [21], compound **19** was thus characterized as 7-hydroxyflavone glucoside. Meanwhile, the remaining node with a precursor ion at m/z 418.207 was identified as the ammonium adduct ion, $[M + NH_4]^+$, of **19** on the basis of similar fragment ions observed at m/z 239, 221, 137, 109, and 93.

Dihydroxyflavones

Analysis of the MS/MS fragmentation pattern for the nodes in Clusters C and O (Figure 3) suggested that the compounds were the 5,7-dihydroxyflavone (also known as chrysin (**20**)) and its acylated derivatives (**21** and **25**). The node with a precursor ion at m/z 255.123 $[M + H]^+$ (**20**) exhibited fragment ions at m/z 237 for $[(M+H)\text{-}H_2O]^+$, 209 for $[(M+H)\text{-}H_2O\text{-}CO]^+$, and 153 for $[(M+H)\text{-}(^{1,3}B \text{ cleavage})]^+$, with the latter fragment ion having higher relative abundance. This fragmentation pattern was found similar to that of previously reported data for chrysin [22]. Moreover, based on its MS/MS spectrum, obtained in this present study, the additional fragment ion exhibited at m/z 177 for $[(M+H)\text{-}C_6H_5\text{-}H]^+$, which is attributed to a direct loss of ring-B via homolytic cleavage, and the migration of the hydrogen atom at C-3 (hydrogen atom abstraction) to the resulting ring-B further confirmed that the dihydroxyl substitution was both on ring-A (Figure S7). The presence of **20** was also supported by the MS/MS data in negative ion mode with the

precursor ion $[M - H]^-$ at m/z 253.108, which yielded fragment ions at m/z 175 for $[(M-H)\text{-}C_6H_5\text{-}H]^-$ and 151 for $[(M-H)\text{-}(^{1,3}B$ cleavage$)]^-$.

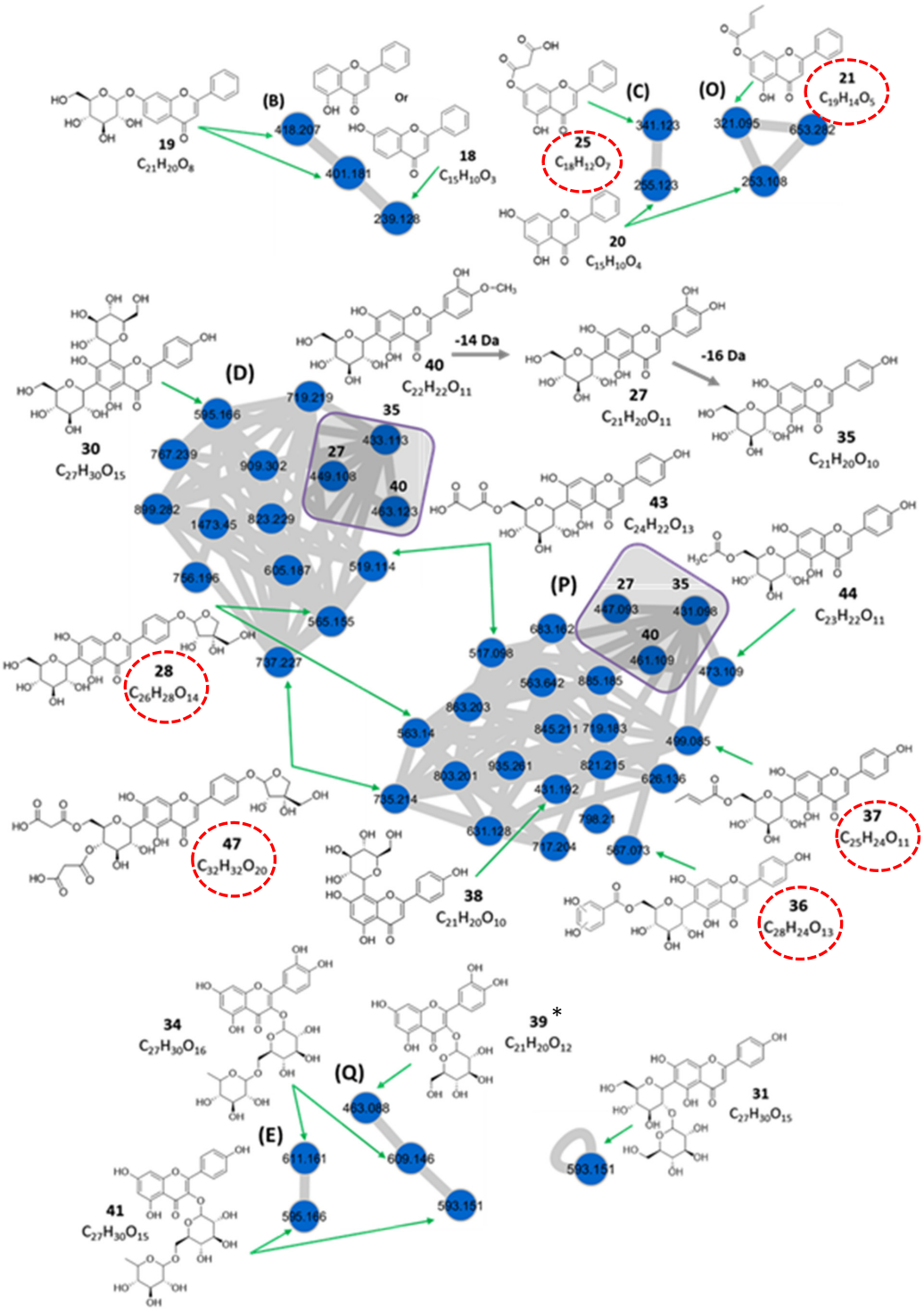

Figure 3. Molecular family of flavonoids: monohydroxyflavones (Cluster B: positive ion), dihydoxyflavones (Cluster C: positive ion, and Cluster O: negative ion), *C*-glycosylflavone derivatives (Cluster D: positive ion, and Cluster P: negative ion), flavonol-3-*O*-glycosides (Cluster E: positive ion, and Cluster Q: negative ion), and flavone-*C*,*O*-diglycoside ("self-loop" node: negative ion), extracted from the full molecular networking (MN) of *Christia vespertilionis* leaf. Red dotted circles represent proposed new structures. * Compound previously reported in *Christia vespertilionis*.

Identical MS/MS features with that of **20** in negative ion mode, i.e., at m/z 253 for [(M−H)-crotonyl]$^-$, 175 for [(M−H)-crotonyl-C_6H_5-H)]$^-$, and 151 for [(M−H)-crotonyl-(^{1,3}B cleavage)]$^-$, were observed in the MS/MS spectrum of another compound that was represented by the node with the precursor ion [M − H]$^-$ at m/z 321.095. This compound had a mass difference of 68 Da (C_4H_4O) from that of **20** and was proposed to be a crotonylated derivative of **20**. Furthermore, a protonated molecular ion, [M + H]$^+$, at m/z 341.123, having a mass difference of 86 Da ($C_3H_2O_3$) from that of **20**, could be suggested as a malonylated derivative of **20**. This compound exhibited similar MS/MS data as **20**, i.e., at m/z 237 for [(M+H)-malonyl-H_2O]$^+$, 177 for [(M+H)-malonyl-C_6H_5-H)]$^+$, and 153 for [(M+H)-malonyl-(^{1,3}B cleavage)]$^+$. The existence of a fragment ion at m/z 237 for [(M+H)-malonyl-H_2O]$^+$ indicated that the most feasible site for the attachment of the malonyl group is to one of the hydroxyl groups on ring-A. On the basis of these results and in accordance with the fact that the attachment of a substituent on ring-A is generally favored at the 7-position due to the involvement of the 5-OH group in intramolecular hydrogen bond formation with the 4-carbonyl group [21], both compounds were characterized as 7-*O*-crotonylchrysin (**21**) and 7-*O*-malonylchrysin (**25**). The proposed fragmentation pathways of **21** and **25** can be found in Figure S8 and Figure S9, respectively.

C-glycosylflavone Derivatives

A detailed inspection of the MS/MS spectral data for Clusters D (positive ion mode), and P (negative ion mode), as shown in Figure 3, also revealed the presence of mono-, di-, and acylated *C*-glycosylflavones. The MS/MS spectral data of the identified compounds were mainly characterized by the neutral losses of 90 and 120 Da, together with the formation of the [aglycone + 12]$^{-\bullet}$ radical fragment ion, which indicates the occurrence of *C*-glycosidic linkage within the parent structure of these compounds. Automated dereplication conducted by GNPS spectral library matching for both Clusters D and P (Figure 3) permitted the annotation of two known mono-*C*-glycosylflavones, namely, luteolin-6-*C*-glucoside (**27**) and apigenin-6-*C*-glucoside (**35**). The nodes with precursor ions at m/z 449.108 [M + H]$^+$ and 447.093 [M − H]$^-$ were annotated as luteolin-6-*C*-glucoside (**27**), commonly known as isoorientin, whereas nodes with precursor ions at m/z 433.113 [M + H]$^+$ and 431.098 [M − H]$^-$ corresponded to apigenin-6-*C*-glucoside (**35**), commonly known as isovitexin. The identity of both compounds was verified as mono-*C*-glycosylflavone based on the existence of fragment ions of [aglycone +71]$^-$, and [aglycone + 41]$^-$, attributable to the neutral losses of 90 and 120 Da, respectively, along with the characteristic fragment ion of [aglycone + 12]$^{-\bullet}$. Furthermore, the attachment of the glucosyl moiety at the C-6 position of the aglycone moiety for these compounds was in agreement with the presence of diagnostic fragment ions for [(M−H)-18]$^-$ in **27** and [(M+H)-4H_2O]$^+$ in **35**, as reported by El Sayed et al. [23] and Abad-García et al. [24], respectively. With a mass difference of 14 Da (CH_2) from that of **27**, the nodes with precursor ions at m/z 463.124 [M + H]$^+$ and 461.109 [M − H]$^-$ in Clusters D and P, respectively, were initially proposed as an *O*-methylated derivative of **35**. Subsequently, the identity of these nodes was elucidated as diosmetin-6-*C*-glucoside (**40**) based on direct comparison of its MS/MS fragmentation pattern in positive ion mode with a previous study by Abad-García et al. [24], in which the existence of a fragment ion at m/z 151 [^{0,2} B]$^+$ specifically justified that the *O*-methylated group was linked to ring-B. An identical fragmentation pattern to **35** was also observed for the spectral node at m/z 431.192 [M − H]$^-$, which allowed its identification as the structural isomer of **35**, known as apigenin-8-*C*-glucoside or vitexin (**38**).

By considering the mass differences of 136, 86, 68, and 42 Da from that of apigenin-6-*C*-glucoside (**35**), five nodes with precursor ions at m/z 567.073 [M − H]$^-$, 519.114 [M + H]$^+$, 517.098 [M − H]$^-$, 499.085 [M − H]$^-$, and 473.109 [M − H]$^-$ were suggested to be the aliphatic and aromatic acyl derivatives of **35**. These mass differences were proposed as dihydroxybenzoyl ($C_7H_4O_3$), malonyl ($C_3H_2O_3$), crotonyl (C_4H_4O), and acetyl (C_2H_2O) groups, which were congruent with the molecular mass of 136, 86, 68, and 42 Da, re-

spectively. The interpretation of their MS/MS fragmentation data in negative ion mode disclosed that these compounds possessed similar MS/MS features as **35**, at m/z 269 for [(M−H)-acylhexose]$^-$, 282 for [aglycone + 12]$^{-\bullet}$, 311 for [(M−H)-acyl-120]$^-$, and 341 for [(M−H)-acyl-90]$^-$. The formation of identical fragment ions at m/z 311 for [(M−H)-acyl-120]$^-$ and 341 for [(M−H)-acyl-90]$^-$ for these compounds were consistent with the attachment of the acyl groups on the hydroxyl part of the sugar unit. An additional fragment ion observed at m/z 413 for [(M−H)-(acyl+H)-OH]$^-$ further indicated the loss of *O*-acyl groups via cleavage from the sugar unit, which specifically refers to the C-6 position of the hexose unit, as shown in Figure 4. Based on these MS/MS fragmentation data, the nodes with precursor ions [M − H]$^-$ at m/z 567.073, 499.085, 517.098, and 473.109 were, therefore, putatively identified as apigenin-6-*C*-(6″-*O*-dihydroxybenzoyl)-glucoside (**36**), apigenin-6-*C*-(6″-*O*-crotonyl)-glucoside (**37**), apigenin-6-*C*-(6″-*O*-malonyl)-glucoside (**43**), and apigenin-6-*C*-(6″-*O*-acetyl)-glucoside (**44**), respectively. The identification of **43** was also further supported by the protonated molecular ion at m/z 519.114 [M + H]$^+$, which exhibited MS/MS data at m/z 415 [(M+H)-(malonyl+H)-OH]$^+$, 313 [(M+H)-malonyl-120]$^+$, and 271 [(M+H)-malonylhexose]$^+$.

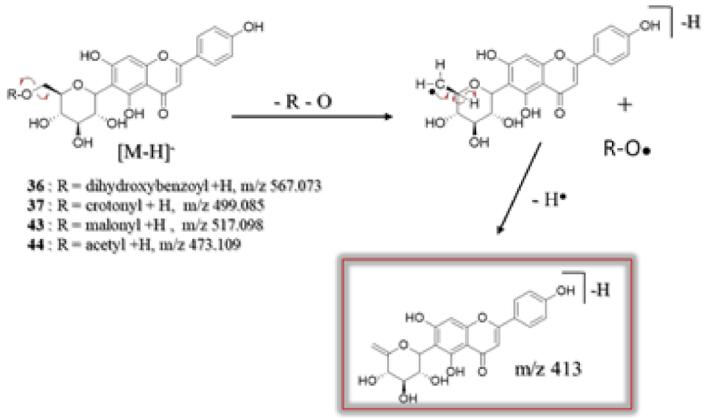

Figure 4. Proposed mechanism for the formation of fragment ion at m/z 413 in acylated derivatives of **35**.

Through a systematic analysis of the MS/MS fragmentation pattern, the nodes with precursor ions at m/z 565.155 [M + H]$^+$ and 563.140 [M − H]$^-$ were characterized as a mono-*C*-glycosylflavone *O*-pentoside. A careful analysis of negative ion mode MS/MS fragmentation data for the spectral node with a precursor ion at m/z 563.140 (Figure S10) revealed that this compound possessed characteristic fragment ions of *C*-glycosidic linkage at m/z 443 for [(M−H)-120]$^-$ and 473 for [(M−H)-90]$^-$, which correspond to the internal cleavage of the sugar moiety. Meanwhile, a direct neutral loss of 132 Da from both the transition ions at m/z 443 and 473 further suggested the presence of one unit of pentosyl moiety ($C_5H_8O_4$) bound to the aglycone molecule via an *O*-linkage. Additional fragment ions exhibited at m/z 269 [aglycone]$^-$ and 282 [aglycone + 12]$^{-\bullet}$ provided information regarding the aglycone unit (apigenin) and the presence of *C*-glycosidic linkage in this compound, respectively. Aided by NMR spectral data (detailed in Section 3.2), the linkages of this compound were confirmed to be positioned at C-6 and 4′-OH of the aglycone unit. Moreover, the characteristic of the pentosyl moiety was also revealed to be similar to that of apiofuranose on the basis of its NMR spectral data. Therefore, this compound was deduced as the new derivative of **35**, named apigenin-6-*C*-*β*-glucoside 4′-*O*-*α*-apiofuranoside (**28**).

With a mass difference of 172 Da from that of **28**, nodes with precursor ions at m/z 737.229 [M + H]$^+$ and 735.214 [M − H]$^-$ were predicted to be a dimalonylated derivative of **28**. A detailed inspection of the negative ion mode MS/MS fragmentation pattern of this compound (**47**) revealed that it has similar characteristic fragment ions as **28** (Figure S11), which supports that it has a similar chemical scaffold as **28**. The proposed

main fragmentation pathways for both compounds are presented in Figure 5. The fragment ions formed at m/z 473 for $[(M-H)\text{-}90\text{-}86\text{-}86]^-$ and 443 for $[(M-H)\text{-}120\text{-}86\text{-}86]^-$ may have resulted from internal cleavages at position 0,4″ and 0,3′ of the *C*-glucoside moiety, which supports the attachment of each of the malonyl units to the hydroxyl positions of C-4″ and C-6″, respectively. The existence of a fragment ion at m/z 545 for $[(M-H)\text{-}(86+H_2O)\text{-}86]^-$ further indicated the specific cleavage of the two malonyl units at C-4″ and C-6″ of the glucoside unit (Figure 6A). In addition, the significant presence of a fragment ion at m/z 249 $[^{1,3}B]^-$, generated from cleavage at positions 1 and 3 of ring-C, via the RDA mechanism, provided evidence for the presence of an unsubstituted pentosyl moiety, linked to ring-B of the aglycone (Figure 6B). The predicted structure for compound **47** as apigenin-6-*C*-*β*-[(4″,6″-*O*-dimalonyl)-glucoside] 4′-*O*-*α*-apiofuranoside was further verified with the aid of NMR spectral data (detailed in Section 3.2).

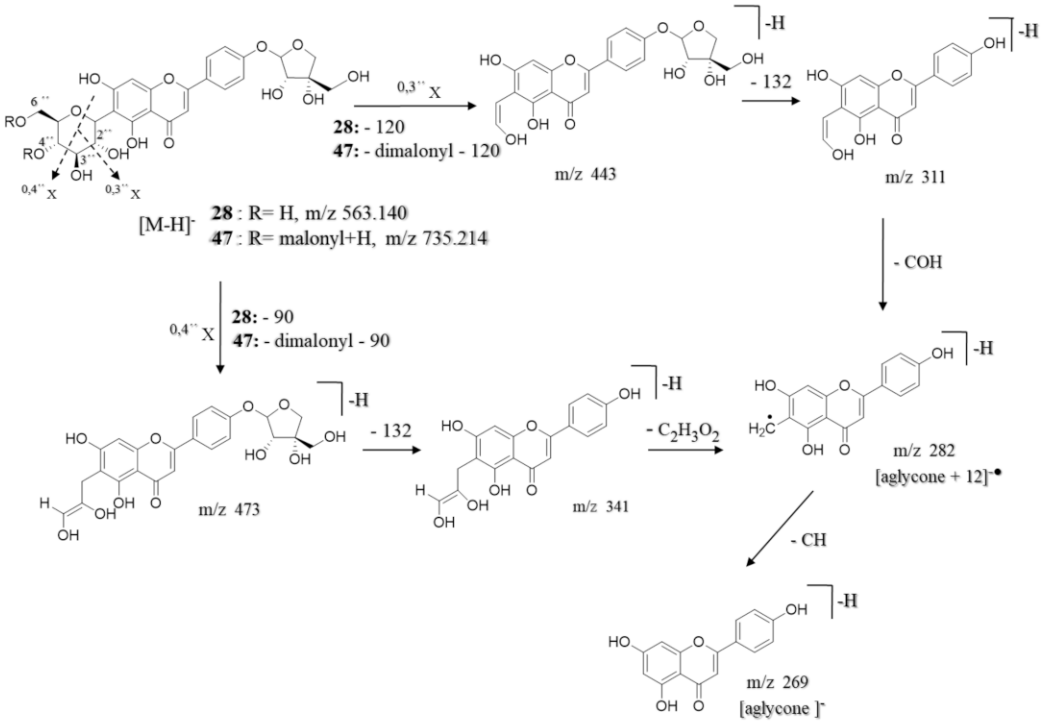

Figure 5. Proposed fragmentation pathways for the major product ions observed in the MS/MS spectra of compound **28** and its dimalonylated derivative (**47**), recorded in negative ion mode.

A node with precursor ion $[M + H]^+$ at m/z 595.166, a mass difference of 162 Da from that of **35**, exhibited characteristic fragment ions at m/z 433 for $[(M+H)\text{-}162]^+$, 337 for $[(M+H)\text{-}120\text{-}120\text{-}H_2O]^+$, and 367 for $[(M+H)\text{-}120\text{-}90\text{-}H_2O]^+$. The two consecutive losses of 120 Da for the m/z 337 ion were suspected to have originated from the simultaneous cleavage of two sugar units, providing evidence for the presence of two hexose units in this molecule. Thus, the molecule was assigned as the di-*C*-glycosylflavone, apigenin-6,8-di-*C*-glucoside (also known as vicenin 2) (**30**) [24].

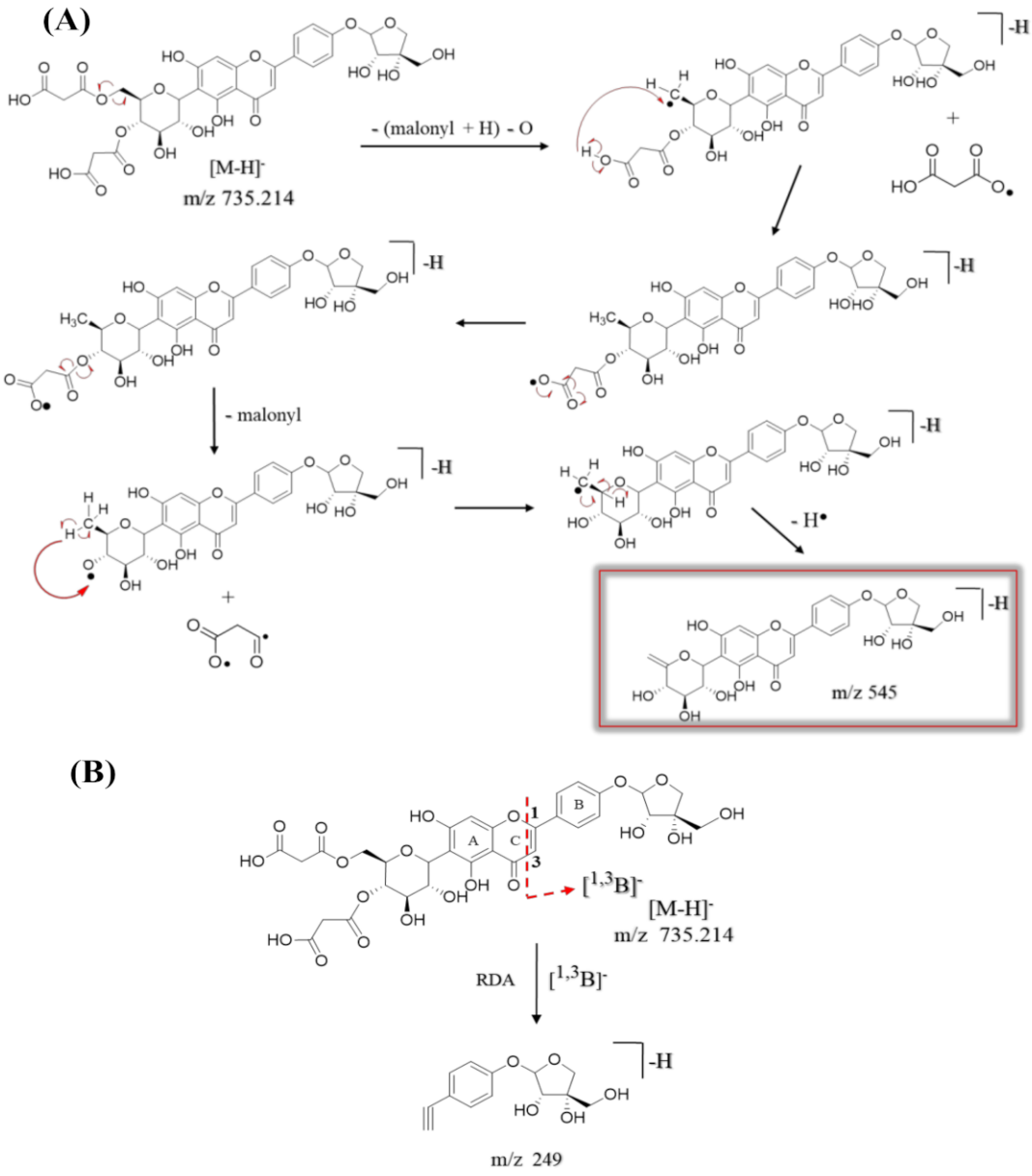

Figure 6. Proposed mechanism for the formation of fragment ions at (**A**) m/z 545 and (**B**) m/z 249 in **47**.

Flavone-*C*,*O*-diglycoside

Compound **31,** with a deprotonated molecular ion at m/z 593.151 $[M - H]^-$, was assigned as apigenin-6-*C*-glucosyl-2″-*O*-glucoside, alternatively known as isovitexin-2″-*O*-glucoside, based on fragment ions observed at m/z 473 for $[(M-H)\text{-}120]^-$, 413 for $[(M-H)\text{-}180]^-$, and 293 for $[(\text{aglycone}+41)\text{-}18]^-$, which indicate the characteristic of flavone *O*-glycosyl-*C*-glucoside (1→2 interglycosidic linkage) [25].

Flavonol-3-*O*-glycosides

In Clusters E (positive ion mode), and Q (negative ion mode), shown in Figure 3, automated GNPS spectral library matching allowed the annotation of several flavonol-3-*O*-glycosides. The nodes with precursor ions at m/z 611.161 $[M + H]^+$ and 609.146 $[M - H]^-$ were annotated as quercetin-3-*O*-rutinoside (rutin) (**34**), while the node with a precursor ion at m/z 463.088 $[M - H]^-$ was annotated as quercetin-3-*O*-glucoside or isoquercitrin (**39**), as previously reported in *C. vespertilionis* [4]. In negative ion mode, these compounds were characterized based on the presence of deprotonated main aglycone product ion $[Y_o]^-$

and also the highly abundant radical aglycone $[Y_o\text{-H}]^{-\bullet}$. These are typical fragmentation patterns observed for the flavonol-3-*O*-glycosides [26], which result from the neutral losses of saccharide or disaccharide moieties $[(M-H)\text{-gly})]^-$ via homolytic and heterolytic cleavages of the glycosidic bond, respectively. Using this information and in comparison with literature data, the remaining compound with precursor ions at *m*/*z* 595.166 $[M + H]^+$ and 593.151 $[M - H]^-$ was deduced to be kaempferol-3-*O*-rutinoside (**41**). In negative ion mode, the existence of fragment ions at *m*/*z* 285 (the main aglycone product ion via elimination of rutinose moiety), 255, 227, and 151 further supported kaempferol as the aglycone moiety [27].

3.1.3. Benzyltetrahydroisoquinoline Alkaloids

Previously, alkaloids were reported to be present in *C. vespertilionis* [4]. The presence of alkaloids in this plant could be closely related to its nitrogen-fixing ability [28], a property which seemed to be characteristic of Fabaceae species, especially for members of Papilionoideae and Mimosoideae [29]. In this present study, a detailed analysis of the MS/MS spectral data for the precursor ions $[M + H]^+$ at *m*/*z* 370.170 and 340.160, mapped in Cluster F (Figure 7), led to their tentative identification as new derivatives of benzyltetrahydroisoquinoline-type alkaloids, **23** and **29**, respectively. The protonated molecular ion of both compounds, $[M + H]^+$, was mainly characterized based on neutral loss of an NHR_1R_2 moiety, R_1 and R_2 being the substituent groups on the nitrogen atom, which is a typical fragmentation pattern observed for isoquinoline-type alkaloids [30]. Based on the formation of the $[(M+H)\text{-}NHHC_4H_7]^+$ fragment ion at *m*/*z* 299 for compound **23** and 269 for compound **29**, the substituents, R_1 and R_2, of both compounds were thus suggested to be H and a butenyl group (C_4H_7, 55 Da). Further detailed inspection of the MS/MS spectral data for compound **23** showed that it exhibited fragment ions at *m*/*z* 145 for $[(M+H)\text{-}NHHC_4H_7\text{-}C_8H_{10}O_3]^+$ (base peak), and 127 for $[(M+H)\text{-}NHHC_4H_7\text{-}C_8H_{10}O_3\text{-}H_2O]^+$, suggesting a benzyltetrahydroisoquinoline structure with a monohydroxylated ring-A and trisubstituted ring-C (the substituents being a hydroxyl and two methoxyl groups). A similar MS/MS fragmentation pattern was also observed in the MS/MS spectrum of compound **29**, which exhibited key fragment ions at *m*/*z* 145 for $[(M+H)\text{-}NHHC_4H_7\text{-}C_6H_6O\text{-}CH_2O]^+$ (base peak) and 127 for $[(M+H)\text{-}NHHC_4H_7\text{-}C_6H_6O\text{-}CH_2O\text{-}H_2O]^+$. These fragments and additional ions at *m*/*z* 175 for $[(M+H)\text{-}NHHC_4H_7\text{-}C_6H_6O]^+$ and 119 for $[(M+H)\text{-}C_{13}H_{19}O_2N]^+$ supported a disubstituted ring-A (one hydroxyl and two methoxyl groups) and a monohydroxylated ring-C for compound **29**. The proposed fragmentation pathways for compounds **23** and **29** are presented in Figures S12 and S13, respectively.

3.1.4. Hydroxyjasmonic Acid Derivatives

Hydroxyjasmonic acid derivatives were also detected in *C. vespertilionis* extract based on Clusters G (positive ion mode) and R (negative ion mode) of the generated MN (Figure 7). Spectral library matching via the GNPS platform allowed the annotation of a node in Cluster G, having precursor ion $[M + NH_4]^+$ at *m*/*z* 406.207, as 3-oxo-2-[5-(hexopyranosyloxy)-pent-2-enyl]-cyclopentaneacetic acid (commonly known as tuberonic acid hexoside) (**24**). The putative identity of **24** was also supported by the negative ion MS/MS data, as represented by the node with precursor ion $[M - H]^-$ at *m*/*z* 387.166, which is congruent with previously reported data [31]. The neighboring node, with a precursor ion at *m*/*z* 408.223 $[M + NH_4]^+$, a mass difference of 2 Da from that of **24**, was proposed as its hydrogenated derivative, **26**, further supported by characteristic fragment ions at *m*/*z* 229 for $[(M+NH_4)\text{-}NH_3\text{-}162]^+$, 211 for $[(M+NH_4)\text{-}NH_3\text{-}162\text{-}H_2O]^+$ (base peak), and 165 for $[(M+NH_4)\text{-}NH_3\text{-}162\text{-}H_2O\text{-}(CO+H_2O)]^+$. The base peak ion provided key evidence for the main backbone chain of this compound (Figure S14). The putative identity of compound **26** was further supported by the negative ion MS/MS data, which gave a deprotonated molecular ion at *m*/*z* 389.182 $[M - H]^-$ and fragment ions at *m*/*z* 209 for $[(M-H)\text{-}162\text{-}H_2O]^-$ and 59 for carboxylate ion, CO_2CH_3. The node in Cluster G, with a precursor ion at *m*/*z* 406.244 $[M + NH_4]^+$, was deduced to be a structural isomer of **24**, possibly differing

in the location of the double bond on the backbone chain. This compound (**33**) showed the same fragment ions as **24**, i.e., at *m*/*z* 209 and 163. Another node in Cluster G, having precursor ion $[M + NH_4]^+$ at *m*/*z* 492.244 (**42**), a mass difference of 86 Da from that of **33**, was proposed to be a malonylated derivative of **33**. The mass spectral data suggested that the malonyl moiety ($C_3H_2O_3$) was attached to the hydroxyl group of the hexoside unit based on the fragment ions formed at *m*/*z* 227 for the simultaneous losses of ammonia and malonylhexose, 209 for $[(M+NH_4)\text{-}NH_3\text{-}162\text{-}86\text{-}H_2O]^+$, and 163 for $[(M+NH_4)\text{-}NH_3\text{-}162\text{-}86\text{-}H_2O\text{-}(CO+H_2O)]^+$. Meanwhile, a node with a precursor ion at *m*/*z* 475.217 was subsequently assigned as the protonated molecular ion $[M + H]^+$ of **42** on the basis of a similar fragmentation pattern at *m*/*z* 227, 209, and 163.

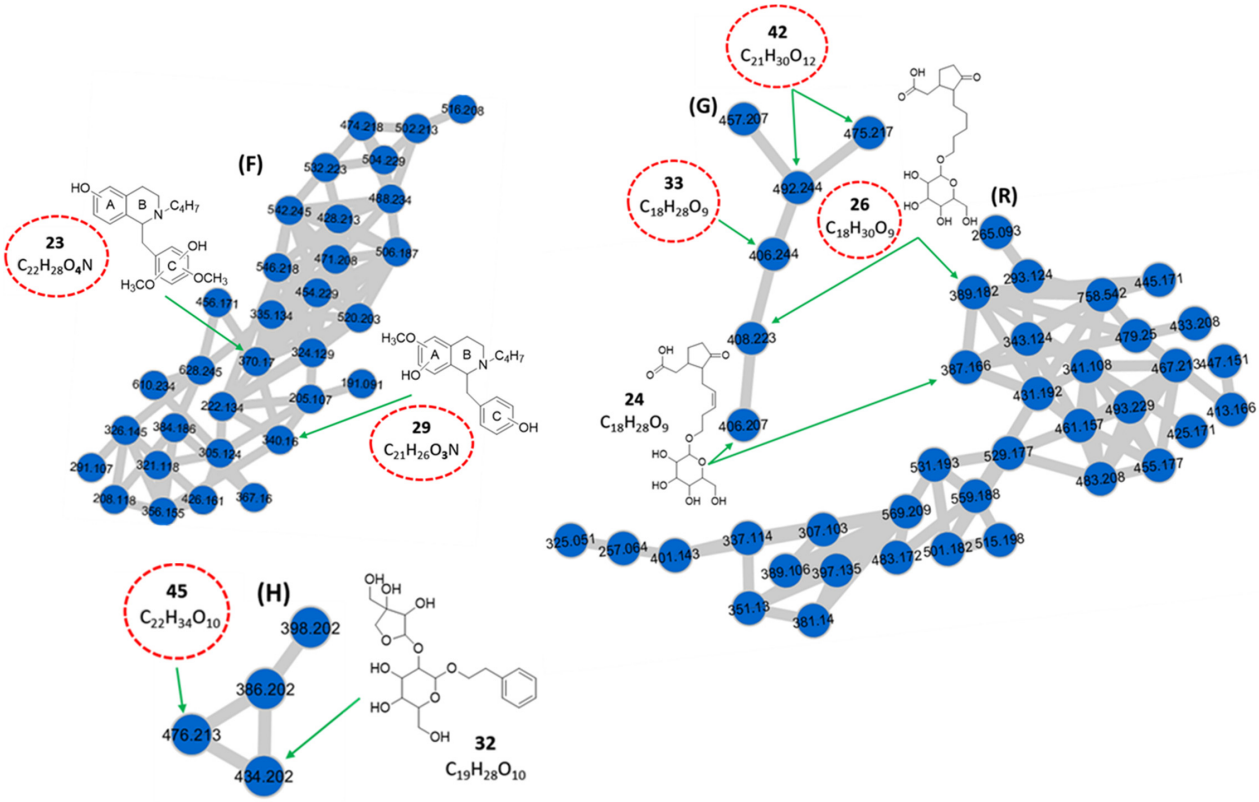

Figure 7. Molecular families of benzyltetrahydroisoquinoline alkaloids (Cluster F: positive ion), hydroxyjasmonic acid derivatives (Cluster G: positive ion, and Cluster R: negative ion), and phenethyl derivatives (Cluster H: positive ion), extracted from the full MN of *Christia vespertilionis* leaf. Red dotted circles represent proposed new structures.

3.1.5. Phenethyl Derivatives

In Cluster H (Figure 7), the node with a precursor ion $[M + NH_4]^+$ at *m*/*z* 434.202 was assigned as phenethyl-1-*O*-*β*-D-apiofuranosyl (1→2)-*β*-D-glucopyranoside (**32**) based on GNPS spectral library matching. The compound, also known as sayaendoside, was previously isolated from young seedpods of *Pisum sativum* L. [32]. From the analysis of its MS/MS spectral data, it was found that **32** exhibited the characteristic fragment ion of 2-phenylethanol as the aglycone unit at *m*/*z* 123 for $[(M+NH_4)\text{-}NH_3\text{-}294]^+$, resulting from direct losses of ammonia and the disaccharide moiety [*β*-D-apiofuranosyl (1→2)-*β*-D-glucopyranoside]. This observation verified that the disaccharide moiety was *O*-linked to the hydroxyl group of the 2-phenylethanol chain. Fragment ions attributable to losses of the disaccharide moiety [*β*-D-apiofuranosyl (1→2)-*β*-D-glucopyranoside] and *β*-D-apiofuranosyl were also observed at *m*/*z* 295 and 133, respectively. Another node in Cluster H had a precursor ion $[M + NH_4]^+$ at *m*/*z* 476.213, a 42 Da (C_3H_6) mass difference from that of **32**. Its MS/MS data showed similar sugar moiety fragment ions to that of

32, at *m*/*z* 295 and 133, indicating that the additional substituent was not attached to the hydroxyl group of the disaccharide moiety. Based on the 2-phenylethanol structure, there was only one active site of the hydroxyl group, which was already linked to the disaccharide moiety. Therefore, it is feasible to suggest that the additional substituent was attached to the 2-phenylethanol chain, either on the phenyl ring or on the saturated carbon chain. Furthermore, a fragment ion that was in agreement with the proposed substituted aglycone structure was observed at *m*/*z* 165 for [(2-phenylethanol)+42 Da]$^+$ (Figure S15). This fragment ion, resulting from the losses of the disaccharide moiety (294 Da) and ammonia, further supported the putative identity of compound **45** as an isopropyl derivative of **32**.

3.1.6. Monoacylglycerols

GNPS spectral library matching allowed the annotation of several monoacylglycerol derivatives in Cluster I (Figure S16). The nodes with precursor ions at *m*/*z* 532.348 [M + NH_4]$^+$ and 353.268 [M + H]$^+$ were annotated as 9,12,15-Octadecatrienoic acid, 3-(hexopyranosyloxy)-2-hydroxypropyl ester (**49**), and 9,12,15-Octadecatrienoic acid, 2,3-dihydroxypropyl ester (1-monolinolenin) (**50**), respectively. The same backbone chain was proposed for both compounds based on their fragment ions at *m*/*z* 353, 261, and 243. The fragment ion observed at *m*/*z* 353 for [(M+NH_4)-NH_3-162)]$^+$ supported the presence of one hexose moiety in the structure of **49**. Meanwhile, an examination of the MS/MS spectral data of neighboring nodes with precursor ions at *m*/*z* 351.254 [M + H]$^+$ and 370.295 [M + NH_4]$^+$ resulted in their putative identification as 6,9,12,15-Octadecatetraenoic acid, 2,3-dihydroxypropylester (**48**) and the [M + NH_4]$^+$ ion of **50**, respectively. The fragmentation pattern of the **48** and **50** exhibited a consistent loss of 92 Da, attributable to the loss of a glycerol moiety ($C_3H_8O_3$), which was observed as base peak ions at *m*/*z* 259 and 261, respectively. The additional loss of a water molecule (H_2O) from both the transition ions at *m*/*z* 259 and 261 gave rise to fragment ions at *m*/*z* 241 and 243, further supporting the assignment of compounds **48** and **50**, respectively.

3.1.7. Fatty Acid Amides

A detailed analysis of Cluster J (see Figure S16) revealed that the compounds assigned to this cluster were fatty acid amides. These compounds produced the main characteristic fragment ions of [(M+H)-NH_3]$^+$, and [(M+H)-NH_3-H_2O]$^+$, which corresponded to the losses of ammonia and water molecules at the carboxamide functional group of these molecules. By comparison of the MS/MS spectral data with the literature [33], the identity of compounds **51**, **52**, **55**, and **60** were annotated as 9,12-octadecadienamide, 9-octadecenamide, 9-eicosenoic acid formamide, and 13-docosenamide, respectively.

3.1.8. Chlorophyll Derivatives

Cluster K (see Figure S17) was identified as that of chlorophylls based on GNPS spectral library matching. The node with precursor ion [M + H]$^+$ at *m*/*z* 593.277 was annotated as pheophorbide-a (**53**), which has been reported in *C. vespertilionis* [4]. This compound displayed key fragment ions at *m*/*z* 533, 459, and 447. The ion at *m*/*z* 533 was derived from the losses of carbomethoxy group at C-13^2 and an additional proton (CO_2CH_3+H), whereas the ion at *m*/*z* 459 indicated the losses of both substituents at C-17 and C-13^2 ($C_5H_{10}O_4$) [34]. Furthermore, through careful analysis of its MS/MS fragmentation, the simultaneous losses of both C-17 ($C_4H_6O_2$) and C-18 (C_2H_4) portions of the molecule, along with the additional losses of the methoxy group and the proton at C-13^2 (OCH_3+H), gave rise to the fragment ion at *m*/*z* 447. With a mass difference of 14 Da (CH_2) higher than that of **53**, the neighboring node with a precursor ion [M + H]$^+$ at *m*/*z* 607.292 was elucidated as an *O*-methylated derivative of **53**. This compound exhibited significant characteristic fragment ions at *m*/*z* 575, 487, and 447, resulting from the losses of both C-17 and C-18 portions of the molecule, together with the losses of the methoxy group and the proton at C-13^2, which were found compatible with the structure of pheophorbide-a

methyl ester (**56**). The MS/MS spectrum of **56** and its proposed fragmentation pathway are presented in Figure S18 and Figure S19, respectively.

3.1.9. Carotenoids

The inspection of MS/MS spectra of the nodes in Cluster L (see Figure S17) revealed that they exhibited characteristic carotenoid fragment ions at m/z 119 and 145, which originate from the fragmentation of the polyene backbone chain via C9-C10 and C13′-C14′ cleavages and C6-C7 and C15-C15′ cleavages, respectively.

The nodes with precursor ions $[M + H]^+$ at m/z 601.424 and 585.430 were characterized as epoxy carotenoids based on the characteristic fragment ions observed at m/z 221, resulting from the C10-C11 cleavage of the polyene chain. The node with a precursor ion $[M + H]^+$ at m/z 601.425 yielded fragment ions at m/z 583 for $[(M+H)-18]^+$ and 521 for $[(M+H)-80]^+$ due to loss of water molecules at one of the hydroxyl group positions and loss of two 5,6-epoxy units, respectively. The absence of a key fragment ion at m/z 393.000 (due to the cleavage of the double bond allylic to the allenic carbon) that would have been observed in neoxanthin [35] led to the conclusion that this carotenoid was, in fact, violaxanthin (**54**), the structural isomer of neoxanthin. The identity of the node with precursor ion at m/z 585.430 $[M + H]^+$ was characterized as antheraxanthin (**58**). Additional fragment ions observed at m/z 567 for $[(M+H)-18]^+$ and 549 for $[(M+H)-18-18]^+$ supported the presence of two hydroxyl groups in compound **58** [36].

Cluster L was also constituted by carotenoids containing both α and β-ionone rings as the end groups (m/z 568.428, $[M]^{\bullet+}$), as well as carbonyl-containing end groups (m/z 367.263, $[M + H]^+$). The node with a precursor ion $[M + H]^+$ at m/z 367.263 was assigned as β-apo-12′-luteinal (**57**) based on the formation of the characteristic fragment ions at m/z 349 for $[(M+H)-18]^+$, due to loss of water molecule at the hydroxyl group position, and at m/z 161, corresponding to a hydroxylated terminal β-ring, resulting from a C10-C11 cleavage. The major product ions observed in the MS/MS spectrum of **57** are presented in Figure S20. Meanwhile, the node with radical cation $[M]^{\bullet+}$ at m/z 568.428, which exhibited a fragment ion at m/z 135, resulting from C7-C8 cleavage, was consistent with the characteristic fragment ion of carotenoids containing a hydroxylated β-ionone ring. On the basis of this information, this node was subsequently identified as lutein (**59**) and was further distinguished from its structural isomer, zeaxanthin, based on the characteristic fragment ion at m/z 430, generated via elimination of the terminal α-ionone ring (138 Da) [37].

3.1.10. Other Compounds

Inspection of the MS/MS spectral data of the peaks that appear in the TICs of both positive and negative ion modes (Figure S1a) also allowed the identification of other miscellaneous compounds, comprising organic acids, a nucleoside, and amino acids. All these compounds appeared as "self-loop" nodes in the generated MN of *C. vespertilionis* leaf.

Compound **1**, with a deprotonated molecular ion $[M - H]^-$ at m/z 195.050, was identified as D-gluconic acid. It displayed fragment ions at m/z 177 for $[(M-H)\text{-}H_2O]^-$, 147 for $[(M-H)\text{-}H_2O\text{-}CH_2O]^-$, 129 for $[(M-H)\text{-}2H_2O\text{-}CH_2O]^-$, and 111 for $[(M-H)\text{-}3H_2O\text{-}CH_2O]^-$ [38]. Compound **3** was putatively characterized as the nucleoside molecule, namely, adenosine, which presented a protonated molecular ion $[M + H]^+$ at m/z 268.104. The MS/MS spectra of this compound exhibited a fragment ion at m/z 136 for $[(M+H)-132]^+$, which corresponded to the formation of the adenine ion, which, in turn, lost a molecule of NH_3 to give to the fragment ion at m/z 119. This fragmentation pattern was in accordance with that reported by Ouyang et al. [39]. Compound **4** showed a deprotonated molecular ion $[M - H]^-$ at m/z 191.019, and fragment ions at m/z 173 for $[(M-H)\text{-}H_2O]^-$, 129 for $[(M-H)\text{-}H_2O\text{-}CO_2]$, and 111 (base peak) for $[(M-H)\text{-}CO_2\text{-}2H_2O]^-$, all of which matched with the characteristic fragment ions of citric acid [38]. Compounds **5**, **8**, and **12**, with protonated molecular ions $[M + H]^+$ at m/z 182.081, 166.086, and 205.097, respectively, were characterized as amino acids based on the common neutral losses of 46, 63, and/or 17 Da, resulting in the formation of main fragment ions, viz., $[(M+H)\text{-}H_2O\text{-}CO]^+$, $[(M+H)\text{-}H_2O\text{-}$

$CO\text{-}NH_3]^+$ and/or $[(M+H)\text{-}NH_3]^+$ in their MS/MS data. Thus, compounds **5**, **8**, and **12** were putatively assigned as tyrosine, phenylalanine, and tryptophan, respectively [40,41].

3.2. Structural Elucidation of Isolated Compounds

From the results of the dereplication process via MN, compounds **28** and **47** (previously described in Section 3.1.2.) were targeted for isolation in order to validate their predicted structures. The selection of these two constituents was mainly based on practical considerations, specifically due to their well-resolved chromatograms and their presence as the major constituents in the methanolic leaf extract of *C. vespertilionis* (Figure S1b). The ethyl acetate fraction containing these two compounds was subjected to semipreparative reversed-phase HPLC (RP-HPLC). As illustrated in Figure 8, the UV spectra of these compounds exhibited similar UV absorption maxima at 271 and 326 nm. These values were typical for flavonoids with a flavone skeleton, reported to show two maximum absorptions in the range of 250–290 and 310–350 nm [22].

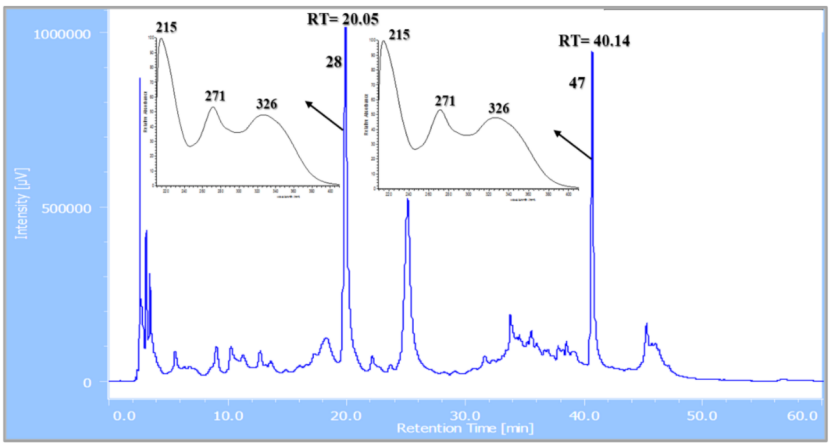

Figure 8. Semipreparative HPLC-PDA chromatogram of ethyl acetate fraction of *Christia vespertilionis* methanolic leaf extract.

Compound **28** was obtained as a light yellow amorphous solid. Its molecular formula was established as $C_{26}H_{28}O_{14}$ based on the deprotonated molecular ion peak observed at m/z 563.140 in negative ion mode ESI-MS/MS spectrum (Figure S10). Its ^{1}H-NMR spectrum (Figures S21 and S22) showed characteristics of a flavonoid diglycoside. An apigenin (4′,5,7-trihydroxyflavone) aglycone was deduced for the compound based on the aromatic proton signals exhibited in the downfield range of δ_H 6.44 to 7.93. The two proton signals at δ_H 7.93 (d, J = 8.9 Hz, H-2′ and H-6′) and δ_H 7.20 (d, J = 8.9 Hz, H-3′ and H-5′), corresponding to the protons on ring-B, were for the ortho-coupled systems between H-2′ and H-3′ and H-5′ and H-6′. The assignment of these protons was further confirmed by correlations observed in the TOCSY spectra (Figure S23). Moreover, the two sets of one proton singlet, resonating at δ_H 6.62 (H-3) and δ_H 6.44 (H-8), further indicated the unsubstituted C-3 and C-8 positions. The occurrence of two units of sugar moiety attached to the aglycone was deducible from the presence of two anomeric protons at δ_H 4.91 (1H, d, H-1″) and δ_H 5.69 (1H, d, H-1). The large J value (9.9 Hz) for the anomeric proton at δ_H 4.91 and the small J value (3.0 Hz) for the anomeric proton at δ_H 5.69 indicated β- and α-configurations for the sugar units, respectively. Complete assignment of the remaining resonance of the aglycone unit and the specific site for the linkage to both sugar units were achieved with the aid of HSQC and HMBC spectral data (Figures S24 and S25). The attachment of one sugar unit at position C-6 was confirmed from the HMBC correlations observed between the anomeric proton at δ_H 4.91 (H-1″) to C-6 (δ_C 108.43, ^2J), C-5 (δ_C 160.62, ^3J), and C-7 (δ_C 167.48, ^3J). For the other sugar unit, HMBC correlation observed between the anomeric proton at δ_H 5.69 (H-1‴) to C-4′ (δ_C 160.17) indicated that the sugar unit was *O*-linked to C-4′ on the aglycone. Careful analyses of the

proton and carbon resonances arising from both sugar units, with the combination of HSQC and HMBC correlations, revealed the presence of *β*-glucose and *α*-apiofuranose as the sugar moieties (Figures S24–S26). The assignment of all protons of the two sugar moieties was also confirmed based on TOCSY spectral data (Figures S27 and S28). The attachment of the *α*-apiofuranose moiety to ring-B of the apigenin unit was further supported by the TOCSY experiment, which showed the spin system between H-1‴ (δ_H 5.69) and the protons of ring-B at δ_H 7.20 (H-3′, H-5′) and δ_H 7.93 (H-2′ and H-6′) (Figure S27). The completely assigned NMR data of **28** is shown in Table 2. Based on the spectral evidence, the structure of **28** was elucidated as apigenin-6-*C*-*β*-glucoside 4′-*O*-*α*-apiofuranoside (Figure 9). The characterization of apigenin-6-*C*-*β*-glucoside was also confirmed by comparison of the NMR data with those reported by Peng et al. [42]. Meanwhile, the identity of the pentosyl moiety as apiofuranose was confirmed by comparison with the NMR data reported by Li et al. [43].

Table 2. NMR data of compound **28** (CD_3OD; 700 MHz, δ in ppm).

Position	δ_H, Mult. (*J* in Hz)	δ_C	HMBC		δ_C *	δ_C **
			^2J	^3J		
Apigenin aglycone						
2		163.57			163.32	
3	6.62 s	102.93	C-4, C-2	C-10, C-1′	102.60	
4		182.10			181.73	
5		160.62			160.64	
6		108.43			108.95	
7		167.48			163.32	
8	6.44 s	94.67	C-7, C-9	C-10, C-6	93.79	
9		157.57			156.31	
10		102.57			102.95	
1′		124.37			121.00	
2′	7.93 d (8.9)	127.57	C-3′	C-6′, C-4′, C-2	128.35	
3′	7.20 d (8.9)	116.37	C-4′	C-5′, C-1′	116.01	
4′		160.17			161.32	
5′	7.20 d (8.9)	116.37	C-4′	C-3′, C-1′	116.01	
6′	7.93 d (8.9)	127.57	C-5′	C-4′, C-2′, C-2	128.35	
6-*C*-*β*-glucoside						
1″	4.91 d (9.9)	73.91	C-6, C-2″	C-5, C-7, C-3″, C-5″	73.13	
2″	4.27 m	70.80	C-1″, C-3″		70.52	
3″	3.49 t (8.9)	78.85	C-2″	C-5″, C-1″	78.93	
4″	3.53 m	70.09	C-3″, C-5″	C-6″	70.20	
5″	3.42 m	80.97	C-4″		81.38	
6″ a	3.87 dd (12.0, 2.0)	61.18	C-5″	C-4″	61.37	
6″ b	3.76 dd (12.0, 5.0)					
4′-*O*-*α*-apiofuranoside						
1‴	5.69 d (3.0)	106.96	C-2‴	C-4′, C-4‴, C-3‴		109.10
2‴	4.29 d (3.0)	76.83	C-1‴	C-5‴		75.90
3‴		78.94				78.70
4‴ a	4.14 d (9.8)	74.26	C-3‴	C-1‴, C-5‴, C-2‴		73.30
4‴ b	3.92 d (9.8)					
5‴ a	3.65 d (7.3)	63.05	C-3‴	C-2‴, C-4‴		63.30
5‴ b	3.65 d (7.3)					

* Literature values from Peng et al. [42]. ** Literature values from Li et al. [43].

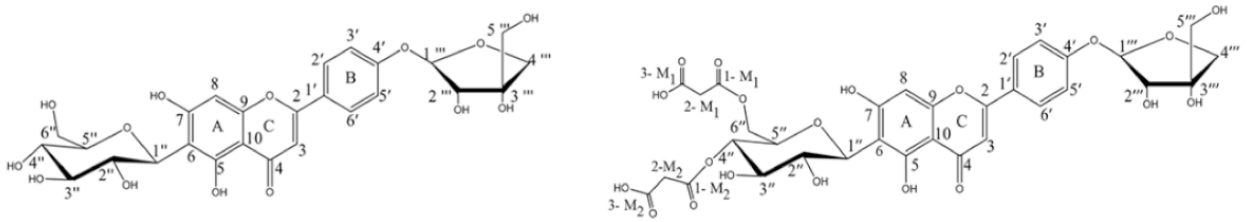

Figure 9. Chemical structures of compounds **28** and **47**.

Compound **47** was obtained as a light yellow amorphous solid. Its molecular formula was determined as $C_{32}H_{32}O_{20}$ based on the deprotonated molecular ion peak observed at m/z 735.214 in negative ion mode ESI-MS/MS spectrum (Figure S11). The ^{1}H-NMR spectrum and the correlations observed in the HSQC and HMBC spectrum, as well as the proton spin system exhibited by the TOCSY experiment on the compound, were found to be similar to those of compound **28**, except for the presence of additional signals attributable to two malonyl units (δ_H 3.80, δ_H 3.71, δ_C 175.21, and δ_C 176.58), in accordance with the structure of a dimalonylated derivative of **28** (Figures S29–S31). Notably, due to the obscuration of the proton signal belonging to the anomeric proton of the *C*-glucoside at δ_H 4.91 (H-1″) by the water resonance, its coupling constant could not be determined. However, since the proton and carbon chemical shifts, as well as the configuration of apiofuranosyl of this compound, were consistent with that of **28**, the anomeric configuration of the *C*-glucoside was thus deduced to be the same as in **28**. A detailed analysis of the HMBC spectral data allowed the assignment of one of the malonyl groups that is O-linked to position C-6″ of the glucoside unit, denoted as M_1. This was deduced from the ^3J correlation observed from H-6″ (δ_H 3.76) to the carbonyl carbon of M_1 at δ_C 175.21 (C_1-M_1) (Figure S31). In addition, two sets of one proton singlet at δ_H 3.80 (H-M_1) and another at δ_H 3.71 (H-M_2) were observed to show correlations with δ_C 175.21 (C_1-M_1), and δ_C 176.58 (C_1-M_2), respectively (Figure S31). These were assigned to the proton signal arising from the methylene protons ($OCOCH_2CO$) of M_1 and M_2, respectively. Instead of appearing as a 2H singlet signal for each of the methylene groups, it was suspected that there was a presence of residual water (D_2O) in the deuterated solvent (CD_3OD), which possibly caused the exchange of one proton in the methylene groups with the deuteron of water to form CHD, resulting in a significant reduction in the integral value of the methylene protons. Correlations between the sugar protons to the carbonyl carbon of M_2 were not observed in the HMBC experiment for some inexplicable reason. To further support the assignment of M_2, information from the ESI-MS/MS analysis, as discussed in Section 3.1.2, was relied on. Moreover, the RP-HPLC elution order and longer elution time for compound **47** (R_T = 40.14) compared to **28** (R_T = 20.05), as shown in Figure 8, suggested a more hydrophobic characteristic for **47**, which was in agreement with the presence of the bulky dimalonyl moieties in its structure. Based on all the information, **47** was identified as apigenin-6-*C*-*β*-[(4″,″-*O*-dimalonyl) glucoside] 4′-*O*-*α*-apiofuranoside (Figure 9).

4. Conclusions

Using MN generated from global MS/MS fragmentation data of its chemical constituents, the present study illustrates the rich chemical diversity of the leaf metabolome of the green-leafed variety of *C. vespertilionis*. A total of 60 metabolites were identified, albeit putatively, comprising phenolic acids, flavonoids (mono- and dihydroxyflavones, *C*-glycosylflavone derivatives, flavone-*C*,*O*-diglycosides, and flavonol-3-*O*-glycosides), benzyltetrahydroisoquinoline alkaloids, hydroxyjasmonic acid derivatives, phenethyl derivatives, monoacylglycerols, fatty acid amides, chlorophyll derivatives, carotenoids, organic acids, nucleoside, and amino acids. Fifty-eight of these compounds are reported for the first time in the leaf metabolome of this plant, including 16 proposed new structures.

Employing mass-targeted isolation, two of the proposed new structures, which were the major constituents of the plant leaves, were successfully purified, and extensive use of 1D and 2D NMR experiments helped characterized the compounds as previously undescribed derivatives of apigenin-6-*C*-*β*–glucoside: apigenin-6-*C*-*β*-glucoside 4′-*O*-*α*-apiofuranoside (**28**) and apigenin-6-*C*-*β*-[(4″,6″-*O*-dimalonyl)-glucoside] 4′-*O*-*α*-apiofuranoside (**47**). In the present literature of *C. vespertilionis*, very little is known about the chemistry of this plant species. There also appears to be no other phytochemical research done on other members of this genus, making it hardly possible to make meaningful comparisons between species of the same genus. Nevertheless, based on the results of this study, it is noteworthy to mention that flavonoids are the major leaf metabolites of this plant. It is highly likely that the high amounts and variety of flavonoid constituents, viz., flavones and flavone glycosides, contribute to the reported biological activity of the plant leaves, at least with respect to its antioxidant property. In addition, the discovery of new derivatives of benzyltetrahydroisoquinoline-type of alkaloids in Cluster F is of chemotaxonomic interest and should be further investigated, considering the pharmacological importance of this class of compounds.

The present study is the first report that provides some valuable detailed insight into the chemistry of the leaf metabolome of the green-leafed variety of *C. vespertilionis*. We envisage that the chemical information obtained through this work will be useful in future phytopharmaceutical research on the plant leaves towards the provision of affordable and quality plant-based health products.

Supplementary Materials: The following are available online at https://www.mdpi.com/article/10.3390/app11083526/s1, Figure S1a: Total ion chromatograms of the leaf methanolic extract of *Christia vespertilionis* in positive and negative ion modes. Figure S1b: Photodiode array chromatogram of the leaf methanolic extract of *Christia vespertilionis.* Figure S2: Proposed fragmentation pathway observed in MS/MS spectrum of *p*-coumaric acid 4-*O*-glucoside (**17**). Figure S3: Proposed fragmentation pathway observed in MS/MS spectrum of the crotonylated derivative of vanillic acid glucosyl ester (**6**). Figure S4: Proposed fragmentation pathway observed in MS/MS spectrum of dihydroxybenzoic acid crotonyl hexoside (**9**). Figure S5: Proposed fragmentation pathway observed in MS/MS spectrum of dihydroxybenzoic acid dimalonyl hexoside (**46**). Figure S6: Proposed fragmentation pathway observed in MS/MS spectrum of 7-hydroxyflavone glucoside (**19**). Figure S7: Proposed fragmentation pathway observed in MS/MS spectrum of 5,7-dihydroxyflavone (also known as chrysin) (**20**). Figure S8: Proposed fragmentation pathway observed in MS/MS spectrum of 7-*O*-crotonylchrysin (**21**). Figure S9: Proposed fragmentation pathway observed in MS/MS spectrum of 7-*O*-malonylchrysin (**25**). Figure S10: Proposed fragmentation pathway observed in MS/MS spectrum of apigenin-6-*C*-*β*-glucoside 4′-*O*-*α*-apiofuranoside (**28**). Figure S11: Proposed fragmentation pathway observed in MS/MS spectrum of apigenin-6-*C*-*β*-[(4″, 6″-*O*-dimalonyl)-glucoside] 4′-*O*-*α*-apiofuranoside (**47**). Figure S12: Proposed fragmentation pathway observed in MS/MS spectrum of benzyltetrahydroisoquinoline derivative (**23**). Figure S13: Proposed fragmentation pathway observed in MS/MS spectrum of benzyltetrahydroisoquinoline derivative (**29**). Figure S14: Proposed fragmentation pathway observed in MS/MS spectrum of the hydrogenated derivative of tuberonic acid hexoside (**26**). Figure S15: Proposed fragmentation pathway observed in MS/MS spectrum of isopropyl derivative of phenethyl-1-*O*-*β*-D-apiofuranosyl (1→2)-*β*-D-glucopyranoside (**45**). Figure S16: Molecular families of monoacylglycerols and fatty acid amides. Figure S17: Molecular families of chlorophyll derivatives and carotenoids. Figure S18: MS/MS spectrum of pheophorbide-a methyl ester (**56**). Figure S19: Proposed fragmentation pathway observed in MS/MS spectrum of pheophorbide-a methyl ester (**56**). Figure S20: Major fragment ions from the fragmentation of *β*-apo-12′-luteinal (**57**). Figure S21: ^{1}H-NMR spectrum of apigenin-6-*C*-*β*-glucoside 4′-*O*-*α*-apiofuranoside (**28**) (700 MHz, in CD_3OD). Figure S22: Expanded ^{1}H-NMR spectrum of sugar signals in apigenin-6-*C*-*β*-glucoside 4′-*O*-*α*-apiofuranoside (**28**) (700 MHz, in CD_3OD). Figure S23: Expanded TOCSY spectrum of apigenin-6-*C*-*β*-glucoside 4′-*O*-*α*-apiofuranoside (**28**) (700 MHz, in CD_3OD). Figure S24: HSQC spectrum of apigenin-6-*C*-*β*-glucoside 4′-*O*-*α*-apiofuranoside (**28**) (700 MHz, in CD_3OD). Figure S25: Expanded HMBC spectrum of apigenin-6-*C*-*β*-glucoside 4′-*O*-*α*-apiofuranoside (**28**) (700 MHz, in CD_3OD). Figure S26: Expanded HMBC spectrum of apigenin-6-*C*-*β*-glucoside 4′-*O*-*α*-apiofuranoside (**28**) (700 MHz, in CD_3OD). Figure S27: Expanded TOCSY spectrum of apigenin-6-*C*-*β*-

glucoside 4′-*O*-*α*-apiofuranoside (**28**) (700 MHz, in CD_3OD). Figure S28: Expanded TOCSY spectrum of apigenin-6-*C*-*β*-glucoside 4′-*O*-*α*-apiofuranoside (**28**) (700 MHz, in CD_3OD). Figure S29: ^{1}H-NMR spectrum of apigenin-6-*C*-*β*-[(4″,6″-*O*-dimalonyl)-glucoside] 4′-*O*-*α*-apiofuranoside (**47**) (700 MHz, in CD_3OD). Figure S30: Expanded ^{1}H-NMR spectrum of sugar signals in apigenin-6-*C*-*β*-[(4″, 6″-*O*-dimalonyl)-glucoside] 4′-*O*-*α*-apiofuranoside (**47**) (700 MHz, in CD_3OD). Figure S31: HMBC spectrum of apigenin-6-*C*-*β*-[(4″,6″-*O*-dimalonyl)-glucoside] 4′-*O*-*α*-apiofuranoside (**47**) (700 MHz, in CD_3OD).

Author Contributions: Conceptualization, K.S. and S.M.M.F.; investigation, A.I.N.; supervision, K.S. and S.M.M.F.; formal analysis, A.I.N.; validation, K.S., S.M.M.F., and S.Y.L.; data curation, K.S., S.M.M.F., S.Y.L., and A.I.N.; writing—original draft preparation, A.I.N.; writing—review and editing, K.S., S.M.M.F., and S.Y.L. All authors have read and agreed to the published version of the manuscript.

Funding: This research received no external funding.

Institutional Review Board Statement: Not applicable.

Informed Consent Statement: Not applicable.

Data Availability Statement: Not applicable.

Acknowledgments: The authors wish to thank Universiti Putra Malaysia for the research facilities. A.I.N. acknowledges the Public Services Department (JPA), Malaysia, for the provision of a study scholarship.

Conflicts of Interest: The authors declare no conflict of interest.

References

1. Ismail, S.; Mokhtar, S. The antecedents of herbal product actual purchase in Malaysia. *Manag. Sci. Lett.* **2015**, *5*, 771–780. [CrossRef]
2. Hudson, A.; Lopez, E.; Almalki, A.J.; Roe, A.L.; Calderón, A.I. A Review of the Toxicity of Compounds Found in Herbal Dietary Supplements. *Planta Med.* **2018**, *84*, 613–626. [CrossRef]
3. Aziz, Z.; Tey, N.P. Herbal medicines: Prevalence and predictors of use among Malaysian adults. *Complement. Ther. Med.* **2009**, *17*, 44–50. [CrossRef]
4. Dash, G. An appraisal of *Christia vespertilionis* (L.F.) bakh. F.: A promising medicinal plant. *Int. J. Pharmacogn. Phytochem. Res.* **2016**, *8*, 1037–1039.
5. Hofer, D.; Schwach, G.; Tabrizi-Wizsy, N.G.; Sadjak, A.; Sturm, S.; Stuppner, H.; Pfragner, R. *Christia vespertilionis* plant extracts as novel antiproliferative agent against human neuroendocrine tumor cells. *Oncol. Rep.* **2013**, *29*, 2219–2226. [CrossRef] [PubMed]
6. Nguyen-Pouplin, J.; Tran, H.; Tran, H.; Phan, T.A.; Dolecek, C.; Farrar, J.; Tran, T.H.; Caron, P.; Bodo, B.; Grellier, P. Antimalarial and cytotoxic activities of ethnopharmacologically selected medicinal plants from South Vietnam. *J. Ethnopharmacol.* **2007**, *109*, 417–427. [CrossRef]
7. Abd Mutalib, N.; Abd Latip, N. Synergistic Interactions between *Christia Vespertilionis* Leaves Extract and Chemotherapy Drug Cyclophosphamide on WRL-68 Cell Line. *Asian J. Pharm. Res. Dev.* **2019**, *7*, 109–113.
8. Lee, J.J.; Saiful Yazan, L.; Kassim, N.K.; Che Abdullah, C.A.; Esa, N.; Lim, P.C.; Tan, D.C. Cytotoxic Activity of *Christia vespertilionis* Root and Leaf Extracts and Fractions against Breast Cancer Cell Lines. *Molecules* **2020**, *25*, 2610. [CrossRef] [PubMed]
9. Upadhyay, H.C.; Sisodia, B.S.; Cheema, H.S.; Agrawal, J.; Pal, A.; Darokar, M.P.; Srivastava, S.K. Novel Antiplasmodial Agents from *Christia vespertilionis*. *Nat. Prod. Commun.* **2013**, *8*, 1591–1594. [CrossRef]
10. Murugesu, S.; Perumal, V.; Balan, T.; Fatinanthan, S.; Khatib, A.; Arifin, N.J.; Shukri, N.S.S.M.; Saleh, M.S.M.; Hin, L.W. The investigation of antioxidant and antidiabetic activities of *Christia vespertilionis* leaves extracts. *S. Afr. J. Bot.* **2020**, *133*, 227–235. [CrossRef]
11. Mohd Yasin, Z.N.; Zakaria, M.A.; Nik Mat Zin, N.N.I.; Ibrahim, N.; Mohamad, F.S.; Mat Desa, W.N.S.; Sul'ain, M.D.; Abu Bakar, N. Biological activities and GCMS analysis of the methanolic extract of *Christia vespertilionis* (L.F.) Bakh. F. leaves. *Asian J. Med. Biomed.* **2020**, *4*, 78–88. [CrossRef]
12. Aguilar-mogas, A.; Sales-pardo, M.; Navarro, M.; Guimerà, R.; Yanes, O. iMet: A network-based computational tool to assist in the annotation of metabolites from tandem mass spectra. *Anal. Chem.* **2017**, *89*, 3474–3482. [CrossRef] [PubMed]
13. Ridder, L.; van der Hooft, J.J.J.; Verhoeven, S.; de Vos, R.C.H.; van Schaik, R.; Vervoort, J. Substructure-based annotation of high-resolution multistage MS^n spectral trees. *Rapid Commun. Mass Spectrom.* **2012**, *26*, 2461–2471. [CrossRef] [PubMed]
14. Ridder, L.; van der Hooft, J.J.J.; Verhoeven, S. Automatic Compound Annotation from Mass Spectrometry Data Using MAGMa. *Mass Spectrom.* **2014**, *3*, 1–7. [CrossRef]

15. Allard, P.; Péresse, T.; Bisson, J.; Gindro, K.; Marcourt, L.; Pham, V.C.; Roussi, F.; Litaidon, M.; Wolfender, J. Integration of Molecular Networking and *In-Silico* MS/MS Fragmentation for Natural Products Dereplication. *Anal. Chem.* **2016**, *88*, 3317–3323. [CrossRef]
16. Quinn, R.A.; Nothias, L.F.; Vining, O.; Meehan, M.; Esquenazi, E.; Dorrestein, P.C. Molecular Networking as a Drug Discovery, Drug Metabolism, and Precision Medicine Strategy. *Trends Pharmacol. Sci.* **2017**, *38*, 143–154. [CrossRef]
17. Yang, J.Y.; Sanchez, L.M.; Rath, C.M.; Liu, X.; Boudreau, P.D.; Bruns, N.; Glukhov, E.; Wodtke, A.; de Felicio, R.; Fenner, A.; et al. Molecular Networking as a Dereplication Strategy. *J. Nat. Prod.* **2013**, *76*, 1686–1699. [CrossRef]
18. Lee, E.M.; Lee, S.S.; Chung, B.Y.; Cho, J.-Y.; Lee, I.C.; Ahn, S.R.; Jang, S.J.; Kim, T.H. Pancreatic Lipase Inhibition by *C*-Glycosidic Flavones Isolated from *Eremochloa ophiuroides*. *Molecules* **2010**, *15*, 8251–8259. [CrossRef]
19. Hirota, B.C.K.; Miyazaki, C.M.S.; Mercali, C.A.; Verdan, M.C.; Kalegari, M.; Gemin, C.; Lordello, A.L.L.; Miguel, M.D.; Miguel, O.G. *C*-glycosyl flavones and a comparative study of the antioxidant, hemolytic and toxic potential of *Jatropha multifida* leaves and bark. *Int. J. Phytomed.* **2012**, *4*, 1–5.
20. Mekky, R.H.; del Contreras, M.M.; El-Gindi, M.R.; Abdel-Monem, A.R.; Abdel-Sattar, E.; Segura-Carretero, A. Profiling of phenolic and other compounds from Egyptian cultivars of chickpea (*Cicer arietinum* L.) and antioxidant activity: A comparative study. *RSC Adv.* **2015**, *5*, 17751–17767. [CrossRef]
21. Cuyckens, F.; Claeys, M. Mass spectrometry in the structural analysis of flavonoids. *J. Mass Spectrom.* **2004**, *39*, 1–15. [CrossRef]
22. Tsimogiannis, D.; Samiotaki, M.; Panayotou, G.; Oreopoulou, V. Characterization of Flavonoid Subgroups and Hydroxy Substitution by HPLC-MS/MS. *Molecules* **2007**, *12*, 593–606. [CrossRef]
23. El Sayed, A.M.; Ezzat, S.M.; El Naggar, M.M.; El Hawary, S.S. In vivo diabetic wound healing effect and HPLC–DAD–ESI–MS/MS profiling of the methanol extracts of eight *Aloe* species. *Rev. Bras. Farmacogn.* **2016**, *26*, 352–362. [CrossRef]
24. Abad-García, B.; Garmón-Lobato, S.; Berrueta, L.A.; Gallo, B.; Vicente, F. New features on the fragmentation and differentiation of *C*-glycosidic flavone isomers by positive electrospray ionization and triple quadrupole mass spectrometry. *Rapid Commun. Mass Spectrom.* **2008**, *22*, 1834–1842. [CrossRef]
25. Negri, G.; Santi, D.D.; Tabach, R. Chemical composition of hydroethanolic extracts from *Siparuna guianensis*, medicinal plant used as anxiolytics in Amazon region. *Rev. Bras. Farmacogn.* **2012**, *22*, 1024–1034. [CrossRef]
26. Kachlicki, P.; Piasecka, A.; Stobiecki, M.; Marczak, L. Structural Characterization of Flavonoid Glycoconjugates and Their Derivatives with Mass Spectrometric Techniques. *Molecules* **2016**, *21*, 1494. [CrossRef] [PubMed]
27. Chen, Y.; Yu, H.; Wu, H.; Pan, Y.; Wang, K.; Jin, Y.; Zhang, C. Characterization and Quantification by LC-MS/MS of the Chemical Components of the Heating Products of the Flavonoids Extract in Pollen Typhae for Transformation Rule Exploration. *Molecules* **2015**, *20*, 18352–18366. [CrossRef] [PubMed]
28. Whiting, P.A. Commercial Production of *Christia subcordata* Moench by Establishing Cultural Practices and by Applying Plant Growth Regulators. The University of Georgia, 2007. Available online: http://athenaeum.libs.uga.edu (accessed on 25 September 2020).
29. Wink, M. Evolution of secondary metabolites in legumes (Fabaceae). *S. Afr. J. Bot.* **2013**, *89*, 164–175. [CrossRef]
30. Qing, Z.; Xu, Y.; Yu, L.; Liu, J.; Huang, X.; Tang, Z.; Cheng, P.; Zeng, J. Investigation of fragmentation behaviours of isoquinoline alkaloids by mass spectrometry combined with computational chemistry. *Sci. Rep.* **2020**, *10*, 733. [CrossRef]
31. Kumar, S.; Chandra, P.; Bajpai, V.; Singh, A.; Srivastava, M.; Mishra, D.K.; Kumar, B. Rapid qualitative and quantitative analysis of bioactive compounds from *Phyllanthus amarus* using LC/MS/MS techniques. *Ind. Crop. Prod.* **2015**, *69*, 143–152. [CrossRef]
32. Murakami, T.; Kohno, K.; Ninomiya, K.; Matsuda, H.; Yoshikawa, M. Medicinal Foodstuffs. XXV. Hepatoprotective Principle and Structures of Ionone Glucoside, Phenethyl Glycoside, and Flavonol Oligoglycosides from Young Seedpods of Garden Peas, *Pisum sativum* L. *Chem. Pharm. Bull.* **2001**, *49*, 1003–1008. [CrossRef]
33. Chua, Y.G.; Bloodworth, B.C.; Leong, L.P.; Li, S.F.Y. Metabolite profiling of edible bird's nest using gas chromatography/mass spectrometry and liquid chromatography/mass spectrometry. *Rapid Commun. Mass Spectrom.* **2014**, *28*, 1387–1400. [CrossRef] [PubMed]
34. Shioi, Y.; Watanabe, K.; Takamiya, K.-I. Enzymatic Conversion of Pheophorbide a to the Precursor of Pyropheophorbide a in Leaves of *Chenopodium album*. *Plant Cell Physiol.* **1996**, *37*, 1143–1149. [CrossRef]
35. Rivera, S.M.; Christou, P.; Canela-Garayoa, R. Identification of carotenoids using mass spectrometry. *Mass Spectrom. Rev.* **2013**, *33*, 353–372. [CrossRef]
36. Li, X.; Lu, M.; Tang, D.; Shi, Y. Composition of Carotenoids and Flavonoids in Narcissus Cultivars and their Relationship with Flower Color. *PLoS ONE* **2015**, *10*, e0142074. [CrossRef]
37. van Breemen, R.B.; Dong, L.; Pajkovic, N.D. Atmospheric pressure chemical ionization tandem mass spectrometry of carotenoids. *Int. J. Mass Spectrom.* **2012**, *312*, 163–172. [CrossRef] [PubMed]
38. Li, S.; Lin, Z.; Jiang, H.; Tong, L.; Wang, H.; Chen, S. Rapid Identification and Assignation of the Active Ingredients in Fufang Banbianlian Injection Using HPLC-DAD-ESI-IT-TOF-MS. *J. Chromatogr. Sci.* **2016**, *54*, 1225–1237. [CrossRef]
39. Ouyang, H.; Li, T.; He, M.; Li, Z.; Tan, T.; Zhang, W.; Li, Y.; Feng, Y.; Yang, S. Identification and Quantification Analysis on the Chemical Constituents from Traditional Mongolian Medicine *Flos scabiosae* Using UHPLC–DAD–Q-TOF-MS Combined with UHPLC–QqQ-MS. *J. Chromatogr. Sci.* **2016**, *54*, 1028–1036. [CrossRef]
40. Piraud, M.; Vianey-Saban, C.; Petritis, K.; Elfakir, C.; Steghens, J.-P.; Morla, A.; Bouchu, D. ESI-MS/MS analysis of underivatised amino acids: A new tool for the diagnosis of inherited disorders of amino acid metabolism. Fragmentation study of 79 molecules of biological interest in positive and negative ionisation mode. *Rapid Commun. Mass Spectrom.* **2003**, *17*, 1297–1311. [CrossRef]

41. Nikolić, D.; Gödecke, T.; Chen, S.-N.; White, J.; Lankin, D.C.; Pauli, G.F.; van Breemen, R.B. Mass spectrometric dereplication of nitrogen-containing constituents of black cohosh (*Cimicifuga racemosa* L.). *Fitoterapia* **2012**, *83*, 441–460. [CrossRef]
42. Peng, J.; Fan, G.; Hong, Z.; Chai, Y.; Wu, Y. Preparative separation of isovitexin and isoorientin from *Patrinia villosa* Juss by high-speed counter-current chromatography. *J. Chromatogr. A* **2005**, *1074*, 111–115. [CrossRef] [PubMed]
43. Li, Y.-L.; Li, J.; Wang, N.-L.; Yao, X.-S. Flavonoids and a New Polyacetylene from *Bidens parviflora* Willd. *Molecules* **2008**, *13*, 1931–1941. [CrossRef] [PubMed]